Zeitschrift: Schweizerische mineralogische und petrographische Mitteilungen = Bulletin suisse de minéralogie et pétrographie

Band: 82 (2002)

Heft: 1

Artikel: Late orogenic evolution of the Variscan lithosphere : Nd isotopic constraints from the western Alps

Autor: Cannic, S. / Lapierre, H. / Monié, P.

DOI: https://doi.org/10.5169/seals-62353

SCHWEIZ. MINERAL. PETROGR. MITT. 82, 77–99, 2002

Late orogenic evolution of the Variscan lithosphere: Nd isotopic constraints from the western Alps

by S. Cannic[1], H. Lapierre[1], P. Monié[2], L. Briqueu[2] and C. Basile[1]

Abstract

We performed geochemical analyses (major- and trace-elements, Nd isotopes) of Late Variscan igneous rocks from the western Alps in order to better constrain the lithospheric evolution at the end of the Variscan orogeny. In the western Alps, the shoshonitic suite from the Croix de Fer pass and the alkaline Combeynot granite were emplaced during the Late Carboniferous. They were followed during the Early Permian by the calc-alkaline diorite porphyries from the "Zone Houillère Briançonnaise", dated by ^{40}Ar–^{39}Ar, and by the calc-alkaline rhyodacites from the Guil valley. These suites postdate the Variscan orogeny and originated in a regime of lithospheric extension and thinning affecting the entire domain of the European Variscan belt. They display subduction-related geochemical features with the exception of the Combeynot granite.

The Croix de Fer suite, the diorite porphyries from the Zone Houillère Briançonnaise and the felsic lavas from the Guil valley show the lowest ($-7 > \varepsilon_{Nd} > -5$) and highest ε_{Nd} values ($+0 > \varepsilon_{Nd} > +2$), respectively. The ε_{Nd} (–2) of the alkaline Combeynot granite is intermediate between those of upper Carboniferous and lower Permian suites. The negative ε_{Nd} of the Upper Carboniferous rocks suggest that they derived from an enriched lithospheric mantle source contaminated by the Hercynian crust. The higher ε_{Nd} of the Early Permian magmas indicate that involvement of this crust decreased with time. Thus, the crustal contribution in the post-orogenic suites disappeared progressively with time at the end of the Variscan orogeny.

Keywords: Permo-Carboniferous, post-orogenic magmatism, trace element chemistry, Nd isotopic composition, western Alps.

1. Introduction

In Europe, the Variscan orogenic belt is characterized during the Permian-Carboniferous times (250–355 Ma; ODIN, 1994) by the development of sedimentary basins coeval with two major plutonic and volcanic cycles. The first cycle is represented by calc-alkaline igneous rocks, emplaced during the Stephanian–Autunian while the second one, Late Permian in age, is alkaline (BROUTIN et al., 1994). Two main mechanisms have been proposed to explain the origin of the calc-alkaline suites: (i) melting of an asthenospheric mantle previously metasomatized by fluids related to oceanic subduction (CABANIS et al., 1990; FINGER and STEYRER, 1990; MERCOLLI and OBERHÄNSLI, 1988; STILLE and BULETTI, 1987), (ii) melting of continental lithosphere, and especially the lower crust, during extension and lithospheric thinning at the end of the Variscan orogeny (INNOCENT et al., 1994). The Permo-Carboniferous igneous rocks exposed in the western Alps represent good candidates to test these two hypotheses.

Several geological, petrological and geochemical studies have been published on the Permo-Carboniferous magmatism from the western Alps (BANZET et al., 1984, 1985; OUAZZANI and LAPIERRE, 1986; MENOT, 1987; OUAZZANI et al., 1987; FINGER and STEYRER, 1990; SCHALTEGGER and CORFU, 1995; DEBON and LEMMET, 1999), the French Massif Central (BRUGUIER et al., 1998) and the Pyrenees (CABANIS and LE FUR-BALOUET, 1989; INNOCENT et al., 1994). However, the sources of the igneous suites from the western Alps are still poorly constrained.

In this paper we present the trace-element and isotopic data of three igneous suites from the western Alps, i.e., shoshonitic lavas of the Croix

[1] LGCA, UMR-CNRS 5025, OSUG, Université Joseph Fourier, Maison des Géosciences, 1381 rue de la Piscine, B.P. 53, F – 38031 Grenoble Cedex, France. <lapierre@ujf-grenoble.fr>
[2] ISTEEM, CC066, Univ. Montpellier II, CNRS, Place Eugène Bataillon, F – 34095 Montpellier Cedex 05, France.

de Fer pass, diorite porphyry sills and dykes of the Zone Houillère Briançonnaise (ZBH) and the alkalic Combeynot granite.

The age and the petrological, geochemical and isotopic characteristics of the three suites will be first discussed. Then these suites will be compared to those of similar age exposed in the central Alps (Italy), in the French Massif Central (Decazeville basin) and in the Pyrenees (Sierra del Cadi basin and Ossau massif).

Finally, the tectonic setting of the three suites will be considered with respect to the geodynamic evolution of the western Variscan belt at the end of its development and before the opening of the Tethyan ocean.

2. Geological and geochemical background

In the western Alps, Late Carboniferous to Early Permian igneous rocks have been indentified in the external crystalline massifs (e.g., Croix de Fer pass, Combeynot massif) and in several places in the "Zone Houillère Briançonnaise" (ZHB): Chardonnet pass, Combarine mine and Guil valley (Fig. 1).

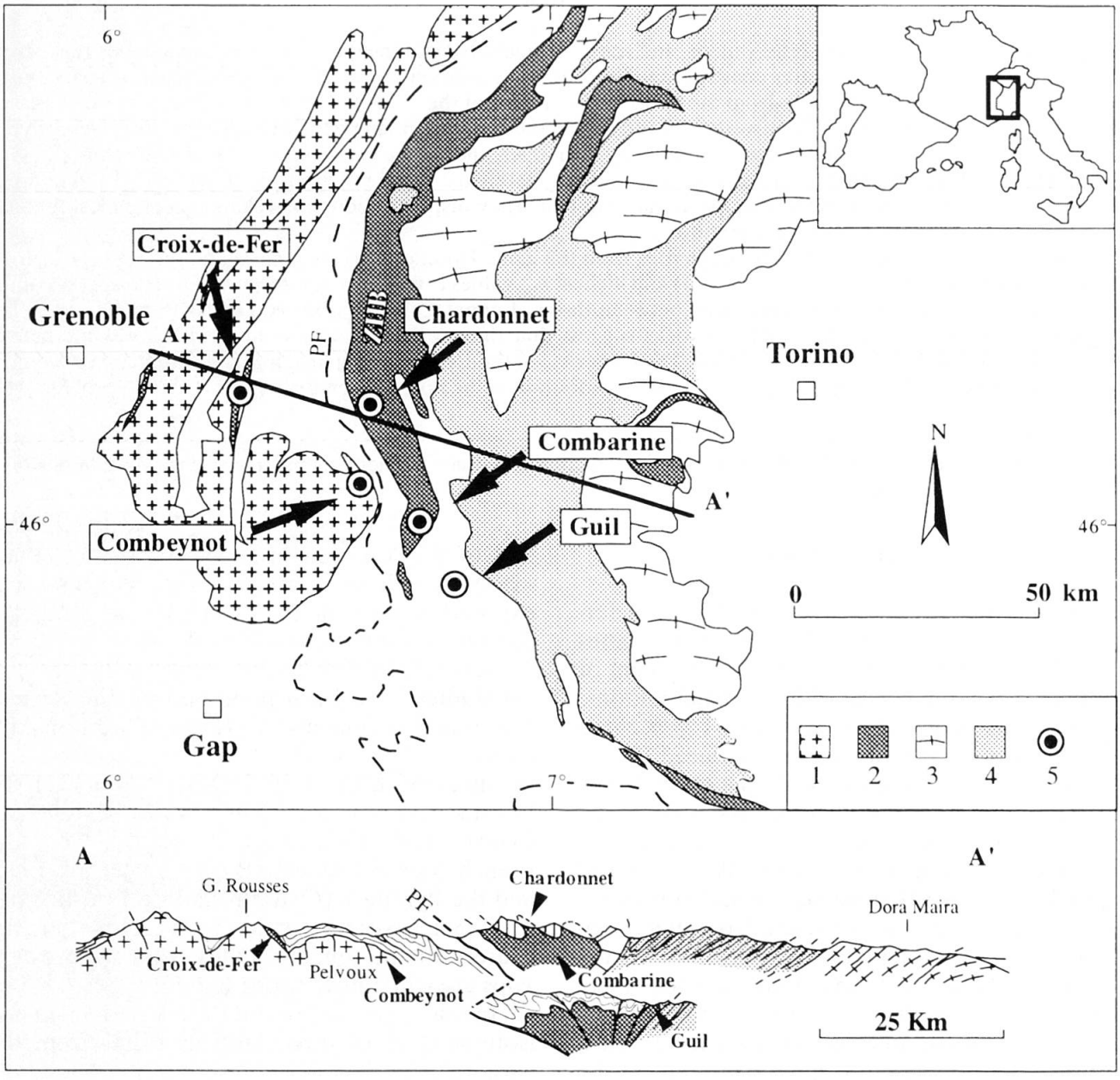

Fig. 1 Simplified geological map and geological section of the western Alps. 1 – External Crystalline Massifs (ECM). 2 – Permo-Carboniferous volcano-sedimentary rocks. 3 – Internal Crystalline Massifs (ICM) and Austro-Alpine units. 4 – Mesozoic ophiolites suites and their sedimentary cover. 5 – Location of the studied Permo-Carboniferous suites. PF – Penninic Front.

2.1. CROIX DE FER SHOSHONITIC SUITE

The volcano-sedimentary suite of the Croix de Fer pass (Grandes Rousses massif, Fig. 1) infills a NNE–SSW graben, which has been inverted during the Alpine collision. The volcanism has been assumed to be Early Stephanian (Late Carboniferous), using paleontologic evidences and facies similarities with the Decazeville basin (LAMEYRE, 1957; GIORGI, 1979; BROUTIN et al., 1994). Recent U–Pb zircon ages of 308 +9/–5 Ma (U. SCHAERER, personal communication) from dacites confirm the paleontologic data. The base of the volcano-sedimentary pile rests unconformably on a pre-Carboniferous basement (Fig. 2), and consists of conglomerates, dacitic breccias and interlayered tuffs locally intruded by basaltic (SiO_2 ~50%, MgO = 8%; BANZET et al., 1985) and andesitic flows and sills (Table 1, BANZET et al., 1985). However, the major part of the volcanic pile is made of andesitic sills and flows interlayered with Carboniferous black shales (BORDET and CORSIN, 1951). OUAZZANI et al. (1987) described two generations of andesites. The quartz-free andesites located just above the basalts include clinopyroxene and amphibole phenocrysts, while those exposed at the top of the pile bear quartz and biotite and are the last lavas to be emplaced. On the basis of petrological and geochemical features, BANZET et al. (1985) considered that the lavas display shoshonitic affinities (MÜLLER et al., 1992) and labelled this suite latite.

The volcanic rocks are affected by low grade metamorphism. Na-rich plagioclase and sanidine are replaced by albite or adularia, while in the mafic rocks, plagioclase is replaced by epidote and quartz. Amphibole, biotite and clinopyroxene are chloritised. Fe–Ti oxides are replaced by sphene.

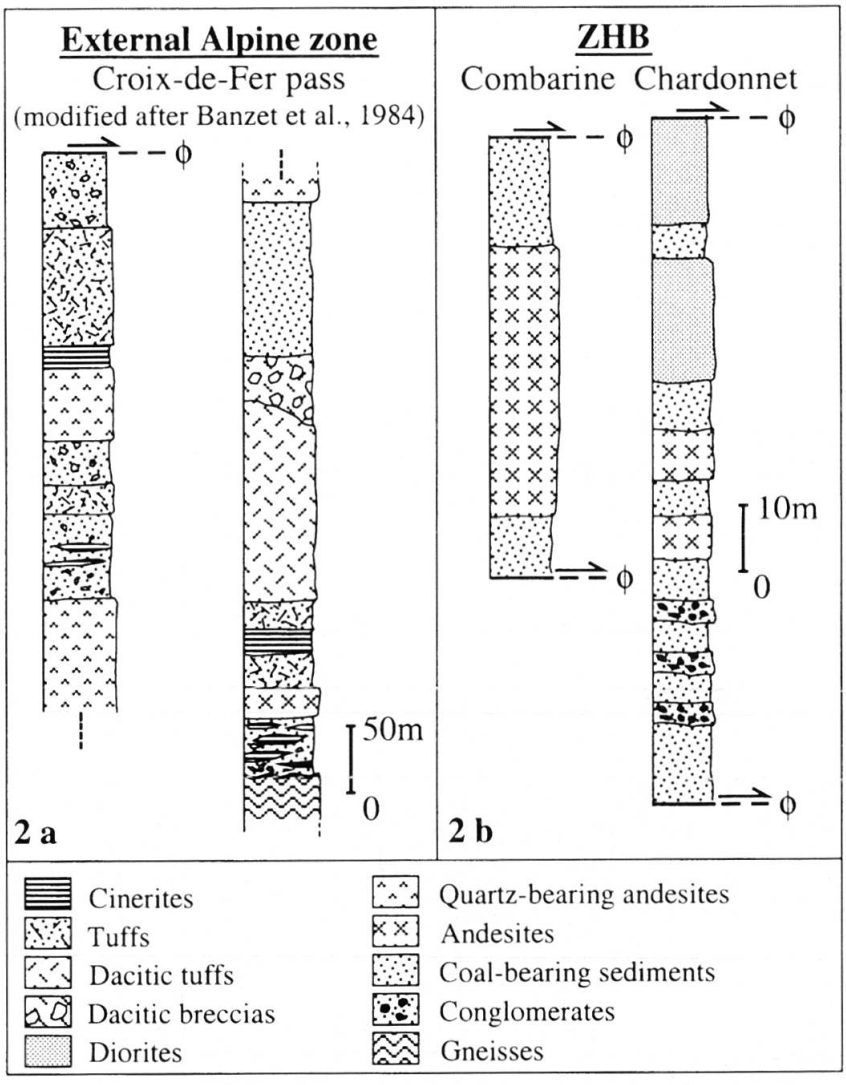

Fig. 2 Stratigraphic columns for the Croix de Fer pass and the Zone Houillère Briançonnaise suites.

Table 1 Location and petrographic characteristics for the Late Carboniferous–Early Permian igneous rocks from the western Alps.

Location	Croix-de-Fer pass	Croix-de-Fer pass	Croix-de-Fer pass	ZHB Combarine	ZHB Chardonnet
Sample	CCF18a/CCF17	CCF4/CCF7	CCF2/CCF20/CCF22	COMB 1 to 3	VIB1/CHAR 6
Name	Latiandesites $53 < SiO_2\% < 55$	Quartz-latiandesites $59.5 < SiO_2\% < 60.5$	Dacites $SiO_2 \sim 64/65\%$	Quartz-diorite $SiO_2 \sim 62/63\%$	Quartz-Andesite $58 < SiO_2\% < 64$
Texture	Porphyritic, fluidal vesicular	Porphyritic trachytic	Highly porphyritic	Fine grained	Porphyritic
Mineralogy	Plagioclase in phenocrysts (20%) and microlites replaced by albite or adularia Cpx (10%) replaced by chlorite Amphiboles (10%) replaced by chlorite + calcite + pyrite Fe-Ti oxides (20%) replaced by titanite zircon, apatite	Clots of plagioclase phenocrysts (30%) rimmed by albite or adularia Quartz phenocrysts (3%) rimmed by calcite Fe-Ti oxides (20%) replaced by titanite zircon, apatite	Abundant and large plagioclase phenocrysts (40%) Acicular amphibole (10%) and biotite (20%) replaced by chlorite Quartz (10%) phenocrysts Fe-Ti oxides (20%) replaced by titanite zircon, apatite	Euhedral plagioclase (40%) replaced by albite and/or sericite ± calcite Euhedral large amphiboles (40%) replaced by chlorite with inclusions of Fe-Ti oxides (5%) replaced by titanite Anhedral quartz (15%)	Clots of plagioclase phenocrysts (30%) replaced albite Euhedral amphibole (30%) replaced by chlorite with Fe-Ti oxides replaced by titanite
Groundmass	Glass replaced by microcristalline quartz chlorite-filled vesicules	Abundant flow-alined plagioclase microlites (60%)	Abundant glass crystallized in microcristalline quartz		Fine grained (40%) with anhedral quartz, zircon and apatite

Location	ZHB Chardonnet	ZHB Chardonnet	Guil	Guil	Combeynot
Sample	CHAR1	CHAR4	GUB1/GUB3/GUB4	GUB5	CO2/CO3/CO5/CO10
Name	Quartz-microdiorite $SiO_2 = 63.5$	Quartz-diorite $SiO_2 = 59\%$	Dacite $SiO_2 = \sim 58\%$	Microdiorite inclusion $SiO_2 = 59\%$	alkali granite $SiO_2 = 74$ to 76%
Texture	Porphyritic	Porphyritic	Porphyritic	Porphyritic	coarse (a) and fine grained (b) porphyritic (a)
Mineralogy	Zoned plagioclase (30%) phenocrysts replaced by albite Preserved pleochroic (40%) Mg-hornblende with preserved Fe-Ti oxides	Euhedral plagioclase (40%) replaced by albite Euhedral large preserved Mg-hornblende (40%) with preserved Fe-Ti oxides (5%) Anhedral quartz (15%)	Quartz and plagioclase phenocrysts (20%) Few Fe-Ti oxides (~5%) replaced by titanite	Zoned plagioclase (30%) phenocrysts replaced by albite and/or sericite Amphibole replaced by chlorite (40%) Fe-Ti oxides replaced by titanite	a) euhedral perthitic microcline + Na-rich plagioclase (57%) subeudral quartz (30%) chloritized biotite magnetite, apatite, zircon and allanite (8 to 10%) b) alkali feldspar (60%), euhedral quartz (36%), rare biotite (3%)
Groundmass	Fine grained (30%) with anhedral quartz, zircon and apatite		Abundant groundmass (80%) crystallized in quartz	Fine grained (30%) with anhedral quartz	

2.2. COMBEYNOT PLUTONIC AND VOLCANIC COMPLEX

The Combeynot complex, located along the eastern boundary of the Pelvoux massif (Fig. 1), comprises acid and mafic igneous rocks, presumably emplaced during the Early Permian (BARBIÉRI, 1970; DEMEULEMEESTER, 1982; BARFÉTY and PÊCHER, 1984). However, recent U/Pb data indicate a Late Carboniferous age of 311 + 6/–5 Ma for the Combeynot granite Ma (U. SCHAERER, personal communication). The Combeynot massif consists of three igneous suites: an acid sheeted dyke complex, a biotite-bearing granite and doleritic dykes (LACOMBE, 1970). The sheeted dyke complex consists of porphyritic microgranite associated with fluidal rhyolite and ignimbrite (COSTARELLA, 1987). The biotite-bearing granite intrudes the pre-Variscan gneiss and forms a roughly concentrically-zoned body. Assuming a cogenetic origin for the microgranite and the granite, COSTARELLA and VATIN-PÉRIGNON (1985) have suggested a rather shallow emplacement for the granite. The dolerites are the last to be emplaced.

The Alpine tectonics affected the acid and mafic rocks of the Combeynot complex by brittle deformation and low-grade metamorphism. This metamorphism is responsible for the replacement of the primary mineralogy by chlorite, albite and sericite. The acid suite exhibits an alkaline affinity (COSTARELLA, 1987). The microgranite and granite are geochemically similar to the Corsican Permian granites (BONIN, 1980, 1982) and show features of within-plate suites (COSTARELLA, 1987).

Table 2 $^{40}Ar/^{39}Ar$ laser probe dates from the Zone Houllière Briançonnaise.

N°	$^{40}Ar^*/^{39}Ar$	$^{36}Ar/^{40}Ar$ x 1000	$^{39}Ar/^{40}Ar$	$^{37}Ar/^{39}Ar$	$^{38}Ar/^{39}Ar$	$\%^{39}Ar$	AGE ± 1sd
VIB1 Amphibole		J=0.016947					
1	1.711	3.141	0.0419	2.103	0.17	12.0	51.6 ± 7.6
2	1.148	3.119	0.0679	3.565	0.09	23.5	34.8 ± 6.4
3	1.778	1.954	0.2375	1.314	0.03	31.1	53.6 ± 4.0
4	5.458	1.91	0.0798	10.453	1.01	38.8	159.6 ± 4.7
5	9.469	0.567	0.0879	13.368	1.69	62.4	268.5 ± 3.7
6	9.722	0.56	0.0858	14.186	1.79	68.2	275.2 ± 3.9
7	9.432	0.085	0.1033	12.907	1.58	71.6	267.5 ± 6.5
8	9.582	0.514	0.0884	14.852	1.8	84.5	271.5 ± 2.9
9	9.5	0.356	0.0941	14.123	1.69	87.6	269.3 ± 7.3
10	9.47	0.682	0.0842	13.958	1.65	100.0	268.5 ± 2.8
					Total age =		194.4 ± 2.4
CHAR1 Amphibole							
1	31.25	2.99	0.0037	21.25	3.59	0.2	766.7 ± 89.7
2	10.452	2.707	0.019	18.321	1.34	1.5	294.2 ± 22.1
3	6.374	1.531	0.0858	5.538	0.28	2.2	185.1 ± 21.6
4	9.580	0.222	0.0974	10.939	0.76	19.8	271.4 ± 3.5
5	9.743	0.202	0.0965	12.234	0.49	55.4	275.7 ± 4.6
6	10.071	0.063	0.0974	12.089	0.41	66.5	284.3 ± 2.4
7	9.957	0.085	0.0978	11.921	0.48	92.9	281.3 ± 2.7
8	9.744	0.158	0.0978	12.964	0.54	97.0	275.7 ± 4.5
9	8.615	0.027	0.1151	10.635	0.43	100.0	245.9 ± 5.3
					Total age =		277.6 ± 3.1
CCF20 Biotite							
1	0.000	3.384	0.0133	0.000	0.09	0.9	0
2	1.151	2.252	0.2904	0.075	0.03	2.9	34.8 ± 5.5
3	1.932	2.111	0.1945	0.041	0.01	6.3	58.1 ± 3.4
4	2.786	1.164	0.2353	0.034	0.01	10.8	83.2 ± 2.1
5	3.761	0.616	0.2174	0.024	0.03	19.4	111.5 ± 1.2
6	4.926	0.267	0.1869	0.025	0.02	35.7	144.7 ± 1.3
7	6.242	0.154	0.1527	0.02	0.00	67.2	181.4 ± 1.3
8	6.091	0.115	0.1585	0.028	0.00	84.3	177.2 ± 1.4
9	4.861	0.244	0.1908	0.041	0.01	88.9	142.8 ± 1.6
10	3.623	0.158	0.263	0.121	0.04	94.0	107.5 ± 1.5
11	4.56	0.122	0.2113	1.389	0.1	100.0	134.3 ± 1.4
					Total age =		147.5 ± 1.4

Table 3 Major- and trace-element analyses for representative igneous samples. Major oxides are in wt%, Fe_2O_3 : total iron as ferric oxide; LOI: loss on ignition. Trace-elements are in ppm. Concentration determined by: (1) XRF (Lyon), 2) ICP-MS and ICP-AES (C.R.P.G.), Nancy, 3) ICP-MS (Toulouse), 4) ICP-MS (Grenoble).

Serie	Standards			Guil valley				Croix–de–Fer pass						
Samples	WS-E	BHVO-1	GA	**GUB 1** Dacite	**GUB 3** Dacite	**GUB 4** Dacite	**GUB 5** Microdioritic inclusion	**CCF2** Dacite	**CCF 4** Quartz-latiandesite	**CCF 7** Quartz-latiandesite	**CCF 17** Latiandesite	**CCF 18a** Latiandesite	**CCF 20** Dacite	**CCF 22** Dacite
Anal.				1		1	1	1	1	1	1	1	1	
SiO_2	–	–	–	57.88	–	58.56	59.69	65.27	60.64	59.56	54.7	52.91	64.47	–
TiO_2	–	–	–	0.63	–	0.62	0.62	0.6	0.88	0.7	0.92	1	0.55	–
Al_2O_3	–	–	–	16.93	–	16.78	16.04	15.66	16.04	15.81	16.77	16.93	15	–
Fe_2O_3	–	–	–	6.1	–	5.75	6.02	4.03	6.61	5.36	7.61	7.15	3.86	–
MnO	–	–	–	0.05	–	0.12	0.11	0.07	0.1	0.13	0.12	0.1	0.07	–
MgO	–	–	–	1.99	–	5.33	5.62	2.47	4.48	2.95	6.81	7.55	1.81	–
CaO	–	–	–	3.32	–	1.99	1.29	1.19	1.07	2.14	2.03	1.3	2.35	–
Na_2O	–	–	–	3.13	–	4.34	3.9	4.04	4.89	3.12	3.78	3.51	3.71	–
K_2O	–	–	–	4.01	–	1.36	1.95	3.86	1.68	5.4	2.88	3.65	3.65	–
P_2O_5	–	–	–	0.14	–	0.14	0.13	0.22	0.21	0.27	0.24	0.29	0.21	–
LOI	–	–	–	5.02	–	4.46	3.91	2.13	2.83	3.36	3.56	3.83	3.47	–
Total	–	–	–	99.2	–	99.45	99.28	99.54	99.43	98.8	99.42	98.22	99.15	–
	4	4	4	3	3	4	3	4	5	4	1	4	4	3	3
Y	32.84	27.86	21.07	14	11.4	17.2	13.3	29.3	29.5	26	20.7	30	33.4	21.8	23.1
Sr	399	402	281	133	182	120	126	136	140	184	229	274	105	118	138
Rb	25.52	9.34	160.9	104	33.6	35.4	38.9	148	129.3	31.0	142	81	99	136	184
Zr	204.1	182.62	179	91	92	99	85	67	70	147	149	146	183	173	185
Nb	18.41	19.28	12.24	4.03	4.06	4.35	3.35	15.3	14.6	10.7	10	10.8	13.7	13.3	13.7
Cu	–	–	–	5.89	5.37	–	6.37	–	–	–	3.9	–	–	4.7	1.75
Ni	–	–	–	18.2	7.52	–	12.2	–	–	–	4.6	–	–	34.8	30.4
Co	44.99	46.23	5.12	10.5	12.4	15.4	12.8	8.74	8.15	13.4	10.6	29.3	19.7	7.24	7.24
Cr	–	–	–	19.5	25.8	–	19.2	–	–	–	17.6	–	–	21.9	7.24
V	–	–	–	149	147	–	157	–	–	–	115	–	–	52	57.6
Sc	–	–	–	45.7	46.6	–	45.9	–	–	–	16.7	–	–	43	46
Zn	–	–	–	28.6	115	–	109	–	–	–	–	–	–	65	56
Ga	–	–	–	17.5	16.8	–	19.4	–	–	–	–	–	–	7.61	16.2
Sn	–	–	–	0.61	0.64	–	0.68	–	–	–	–	–	–	4.41	5.8
Cs	–	–	–	8.4	5.45	–	6.01	–	–	–	–	–	–	9.69	11.18
Ba	334.3	130.11	807	562	266	340	484	920	887	622	762	972	952	1079	1259
				3	3	3	3	4	5	4	4	4	4	3	3
La	26.87	15.45	37.04	13.1	11.8	10.4	10.2	41.3	35.4	18.7	26.6	28.4	40.2	31.7	41.7
Ce	60.92	38.85	76.4	27.1	23.8	21.1	21.7	85.7	74.9	39.8	57.2	56	77.8	67.3	82.8
Pr	7.9	5.49	8.05	3.27	2.85	2.69	2.69	9.85	8.89	4.8	6.84	6.66	9.25	7.99	9.55
Nd	32.74	24.9	27.64	13.5	11.6	10.8	11.2	36.5	33.4	18.2	25.5	26	37.9	31.3	36.5
Sm	8.38	6.07	4.86	2.99	2.53	2.75	2.31	6.91	6.64	3.81	5	5.39	7.88	6.33	6.95
Eu	2.13	2.08	1.09	0.98	0.85	0.94	0.66	1.37	1.15	1.2	1.13	1.47	2.45	0.8	1.09
Gd	6.89	6.2	4.3	3.25	2.56	2.89	2.18	7.33	5.97	4	4.35	5.96	7.79	5.44	5.81
Tb	1.06	0.94	0.61	0.47	0.37	0.48	0.35	1.04	0.86	0.66	0.68	0.93	1.16	0.8	0.86

continued

Dy	6.06	5.21	3.34	2.91	2.38	2.46	2.44	4.62	4.96	4.17	4.01	4.45	5.36	4.72	4.68
Ho	1.17	1	0.68	0.58	0.49	0.51	0.53	0.93	0.98	0.88	0.83	0.94	1.06	0.95	0.92
Er	3.07	2.54	1.93	1.58	1.54	1.43	1.64	2.54	2.7	2.45	2.29	2.59	2.94	2.73	2.63
Tm	–	–	–	0.23	0.2	0.27	0.24	–	–	–	–	–	–	0.42	0.37
Yb	2.57	1.99	1.95	1.54	1.52	1.43	1.67	2.37	2.45	2.1	2.82	2.54	2.9	2.77	2.48
Lu	0.37	0.29	0.309	0.24	0.25	0.22	0.28	0.34	0.36	0.32	0.41	0.38	0.4	0.41	0.36
Hf	5.05	4.58	4.78	2.7	2.83	2.36	2.65	2.02	2.42	3.87	2.91	3.45	4.42	5.25	5.71
Ta	1.16	1.24	1.309	0.29	0.31	0.45	0.26	1.55	1.09	0.66	1.11	1	1.17	1.09	1.07
Tl	–	–	–	0.58	0.26	–	0.3	–	–	–	–	–	–	0.79	0.92
Pb	–	2.64	29.54	10.4	9.3	10.6	7.5	3.55	4.36	1.29	17.6	13.7	3.4	59.2	5.74
Th	2.89	1.11	15.28	2.8	3.07	2.51	2.54	14.5	14.7	5.14	7.4	6.12	9.32	16.7	16.4
U	0.6	0.41	4.63	1.64	1.33	1.25	0.85	3.86	4.03	1.6	2.87	1.73	2.11	4.8	4.94
Zr/Y		–	–	6.5	8.1	5.6	6.4	2.3	2.4	5.7	7.2	4.9	5.5	7.9	8.0
Zr/Nb		–	–	22.6	22.7	22.8	25.4	4.4	4.8	13.7	14.9	13.5	13.4	13.0	13.5
Zr/Th		–	–	32.5	30.0	39.4	33.5	4.6	4.8	28.6	20.1	23.9	19.6	10.4	11.3
(La/Yb)N		–	–	6.1	5.6	5.2	4.4	12.5	10.4	6.4	6.8	8.0	9.9	8.2	12.1
Eu/Eu*		–	–	1.0	1.0	1.0	0.9	0.5	0.6	0.9	0.7	0.8	1.0	0.4	0.5
Eu/Yb		–	–	0.59	0.65	0.67	0.40	0.58	0.47	0.57	0.40	0.59	0.84	0.29	0.44
Ce/Yb		–	–	17.6	15.7	14.8	13.0	36.2	30.6	19.0	20.3	22.0	26.8	24.3	33.4
Ta/Yb		–	–	0.19	0.20	0.31	0.16	0.65	0.44	0.31	0.39	0.39	0.40	0.39	0.43
Th/Yb		–	–	1.82	2.02	1.76	1.52	6.12	6.00	2.45	2.62	2.41	3.21	6.03	6.61

2.3. "ZONE HOULLIÈRE BRIANÇONNAISE" MAGMATISM

The ZHB magmatism consists of diorite porphyries and andesitic dykes and sills (PIANTONE, 1980; OUAZZANI and LAPIERRE, 1986) which intrude Namurian–Westphalian sediments (GREBER, 1965). These rocks are well exposed near the Chardonnet pass and Combarine mines (Fig. 2) and dated as Early Permian (cf. section 4.1).

The ZBH igneous rocks are affected by the Alpine low-grade metamorphism characterized by the following metamorphic assemblage: epidote ± albite ± lawsonite ± prehnite ± pumpellyite ± chlorite (PIANTONE, 1980). However, the magmatic textures and primary mineralogy are often preserved, and more specifically the amphiboles (Table 1). This is the case for the Chardonnet sills. The diorite porphyry is formed of oligoclase and Mg-hornblende phenocrysts. The core of the sills and dykes exhibit microgranular-porphyritic textures, while the margins have microlitic and fluidal textures. Andesite is composed of amphibole phenocrysts and glomero-porphyritic plagioclase clots, which represent a cumulus phase (OUAZZANI et al., 1987). Diorite porphyry and andesite display features of a medium potassic calc-alkaline suite and show geochemical similarities with post-collisionnal magmas (Group IV of HARRIS et al., 1986).

2.4. VALLÉE DU GUIL VOLCANISM

The volcanic rocks of the Guil valley are exposed in a tectonic window beneath the Internal Alpine nappes (Fig. 1). From bottom to top, the volcanic suite consists of rhyolitic flows and breccias, dacites and ignimbrite layers (GOGUEL, 1966). Rhyodacites contain inclusions of andesite and diorite porphyry (see below). The quartz-bearing lavas and their inclusions are affected by a low grade metamorphism similar to that which has affected the other Late Carboniferous and Early Permian igneous rocks. The rocks are undated. However, they are assumed to be coeval with the Lower Permian andesites from Provence (BARFÉTY and PÊCHER, 1984; BROUTIN et al., 1994) on the basis of the calc-alkaline affinity of the volcanic rocks.

3. Analytical techniques

3.1. ^{40}Ar–^{39}Ar DATING

Amphiboles and micas were extracted from an andesite and a microdiorite of the "Zone Houil-

Table 3 (cont.)

Serie	Zone houillère briançonnaise										Combeynot massif					
Sample	VIB 1 Quartz-andesite Whole R.		Amphiboles	COMB 1 Quartz-diorite	COMB 2 Quartz-diorite	COMB 3 Quartz-diorite	CHAR 1 Quartz-microdiorite Whole R.		Amphiboles	CHAR 4 Quartz-diorite	CHAR 6 Quartz-andesite	CO 2		CO 3 Alkali granite	CO 5 Alkali granite	CO 10	
Anal.	1		–	1	1	1	1		–	1	1	1	2	2	2	1	2
SiO_2	58.68		–	61.76	62.73	63.59	52.06		–	59.36	63.89	74.94	74.12	74.93	76.14	76.93	76.16
TiO_2	0.49		–	0.39	0.39	0.37	0.86		–	0.51	0.35	0.18	0.16	0.1	0.08	0.09	0.06
Al_2O_3	16.64		–	16.64	17.02	17.2	17.5		–	17.39	16.55	12.78	12.77	12.86	12.35	11.99	12.02
Fe_2O_3	6.41		–	5.17	5.22	4.57	9.01		–	6.57	5.14	1.88	1.9	1.57	1.23	1.08	1.05
MnO	0.15		–	0.11	0.16	0.11	0.15		–	0.15	0.12	0.03	0.02	Traces	Traces	0.03	Traces
MgO	2.87		–	3.54	3.57	2.12	4.78		–	3.05	1.75	0.78	0.76	0.25	0.2	0.18	0.14
CaO	3.58		–	0.46	0.53	0.95	5.98		–	3.97	2.78	0.17	0.17	0.08	0.26	0.69	0.69
Na_2O	5.95		–	4.58	4.93	6.98	2.92		–	3.44	3.98	2.93	3.05	3.87	3.4	3.19	3.48
K_2O	1.34		–	2.82	2.14	0.81	2.1		–	2.06	2.22	5.01	5.26	4.99	5.06	4.62	4.88
P_2O_5	0.14		–	0.17	0.16	0.15	0.19		–	0.13	0.12	0.04	0.08	0.03	0.03	0.03	0.03
LOI	2.87		–	3.18	2.92	2.12	3.13		–	2.81	3.14	1.04	1.44	1.08	1.06	1.06	1.26
Total	99.12		–	98.82	99.77	98.97	98.68		–	99.44	100.04	99.78	99.73	99.76	99.81	99.89	99.77
	1	4	4	1		3	4	4		4	3	4	3		3	3	
Y	15.7	15.5	51.2	11.4		16.9	22.2	53.4		15.6	10.7	12.8	31.9		22.1	48	–
Sr	245	247	89.8	142	–	250	332	209		253	180	183	72		35.4	27.6	–
Rb	32.9	40.4	1.53	47.5	–	21.6	72	2.78		80	66	76	264		206	277	–
Zr	94	87	–	42.6	–	151	117	–		87	72	62	65		118	81	–
Nb	3.4	4.82	7.08	4.35	–	4.16	4.9	6.21		4.01	4.21	5.71	20.9		21	29.5	–
Cu	5.8	–	–	3.1	–	7.16	10.6	–		–	7.8	–	3.14		5.87	3.99	–
Ni	4	–	–	1.59	–	12.2	8.4	–		–	34	–	1.59		13.4	14.6	–
Co	14.1	14.9	47.1	7.02	–	5.99	21.1	52.3		15.1	8.26	9.6	1.46		0.7	0.97	–
Cr	11.3	–	–	5.8	–	4.96	34	–		–	6.79	–	3.52		1.97	5.31	–
V	112	–	–	56.8	–	54.4	235	–		–	61.9	–	13		2.1	3.8	–
Sc	13.6	–	–	7.6	–	39	27.1	–		–	35.3	–	22.6		29.8	44	–
Zn	–	–	–	89	–	89	–	–		–	37.3	–	21.4		38.9	20.7	–
Ga	–	–	–	16.8	–	14.9	–	–		–	15.1	–	13.8		16	15.4	–
Sn	–	–	–	0.84	–	1.98	–	–		–	0.59	–	4.65		11	3.04	–
Cs	–	–	–	4.32	–	1.47	–	–		–	3.74	–	4.09		4.32	4.62	–
Ba	384	397	56	392		315	273	93		338	400	381	442		288	120	–
	4		4	3		3	4	4		4	3	4	3		3	3	
La	14.7		13.52	15.5	–	17.7	17.9	42.6		16.4	13.5	14.9	25.3		28.8	19.4	–
Ce	30.3		36.7	31.9	–	36.9	38.4	96.2		32.4	27.6	30.4	51.3		56.6	43.6	–
Pr	3.55		5.91	4.24	–	4.51	4.85	12.87		3.93	3.26	3.56	5.89		6.64	5.3	–
Nd	13		29.6	15.6	–	18.1	19.5	55.6		14.9	12.5	13	21.1		24.5	19.8	–
Sm	2.48		8.81	2.81	–	3.71	4.09	12.86		2.98	2.5	2.36	4.81		4.93	5.72	–
Eu	0.77		2.39	0.65	–	0.98	1.18	2.79		0.96	0.83	0.78	0.53		0.37	0.21	–
Gd	2.35		8.8	2.64	–	3.35	3.99	12.39		3.2	2.35	2.16	4.54		4.23	6.5	–
Tb	0.39		1.54	0.42	–	0.49	0.62	1.92		0.48	0.35	0.34	0.86		0.74	1.25	–

continued

Dy		2.44	9.49	2.6	–	3.05	3.73	10.67	2.31	2.14	2.05	6.18	4.74	8.78	–
Ho		0.54	2.06	0.57	–	0.64	0.8	2.21	0.51	0.41	0.45	1.29	1.03	1.85	–
Er		1.55	5.73	1.66	–	2.04	2.25	5.77	1.41	1.27	1.25	4.11	3.19	5.96	–
Tm		–	–	–	–	0.3	–	–	–	0.18	–	0.67	0.53	0.96	–
Yb		1.61	5.77	1.71	–	2.22	2.29	4.6	1.5	1.32	1.29	4.71	3.84	6.84	–
Lu		0.25	0.91	0.27		0.37	0.36	0.66	0.23	0.19	0.21	0.71	0.58	1.06	–
Hf		1.99	–	2	–	4.22	2.59	–	2.19	2.17	1.59	3.36	5.66	3.91	–
Ta		0.36	0.32	0.4	–	0.25	0.42	0.35	0.42	0.34	0.5	2.45	2.58	4.87	–
Tl		–	–	–	–	0.11	–	–	–	0.49	–	1.2	1.58	1.21	–
Pb		20.3	30.8	1.7	–	1.64	8.2	10.98	4.8	7.42	7.69	20.3	9.83	18.5	–
Th		2.99	0.78	4.05	–	4.64	3.78	4.78	4	3.74	3.49	35.2	26.9	42.7	–
U		1.636	2.04	1.18	–	1.78	1.41	0.71	2.16	2.43	2.33	9.54	6.67	8.69	–
Zr/Y	6.0	5.6	–	3.7	–	8.9	5.3	–	5.6	6.7	4.8	2.0	5.3	1.7	–
Zr/Nb	27.6	18.0	–	9.8	–	36.3	23.9	–	21.7	17.1	10.ç	3.1	5.6	2.7	–
Zr/Th		31.4	–	10.5	–	32.5	31.0	–	21.75	19.3	17.8	1.8	4.4	1.9	–
(La/Yb)N		6.5	1.7	6.5	–	5.7	5.6	6.6	7.8	7.3	8.3	3.9	5.4	2.0	–
Eu/Eu*		1.0	0.8	0.7	–	0.9	0.9	0.7	1.0	1.1	1.1	0.4	0.3	0.1	–
Eu/Yb		0.48	0.41	0.38	–	0.44	0.52	0.61	0.64	0.63	0.60	0.11	0.10	0.03	–
Ce/Yb		18.8	6.4	18.7	–	16.6	16.8	20.9	21.6	20.9	23.6	10.9	14.7	6.4	–
Ta/Yb		0.22	0.06	0.23	–	0.11	0.18	0.08	0.28	0.26	0.39	0.52	0.67	0.71	–
Th/Yb		1.86	0.14	2.37	–	2.09	1.65	1.04	2.67	2.83	2.71	7.47	7.01	6.24	–

Table 4 $^{87}Sr/^{86}Sr$ and $^{143}Nd/^{144}Nd$ isotope ratios of the Late Carboniferous–Early Permian igneous rocks. Rb, Sr, Nd and Sm concentrations were determined by ICP-MS (refer to Table 3).

Localisation	Rock	N° Sample	t	Sm	Nd	$^{147}Sm/^{144}Nd$	$^{143}Nd/^{144}Nd$	$\varepsilon(Nd)i$	Rb	Sr	$^{87}Rb/^{86}Sr$	$^{87}Sr/^{86}Sr$	$(^{87}Sr/^{86}Sr)i$	$\varepsilon(Sr)i$
Guil	Dacite	GUB 3	260	2.54	11.6	0.1325	0.512621 ± 3	+ 1.8	33.6	183	0.532	0.70635 ± 5	0.70438	+ 2.7
Guil	Dacite	GUB 1	260	2.99	13.5	0.1336	0.512546 ±07	+ 0.3					0.69940	
Guil	Microdiorite	GUB 5	260	2.31	11.2	0.1248	0.512562 ± 2	+ 0.9	39	126	0.892	0.70634 ± 9	0.70305	– 16
ZHB	Q–diorite	COMB 3	270	3.71	18.1	0.1237	0.512539 ±10	+ 0.6	72	251	0.249	0.70790 ± 1	0.70699	+ 40
ZHB	Q–andesite	VIB 1	270	2.48	13	0.1152	0.512597 ±11	+ 2.0	40	247	0.473	0.70840 ± 3	0.70658	+ 34
ZHB	Amphiboles	VIB 1	270	8.8	29.6	0.1802	0.512702 ±04	+ 1.8	1.53	90	0.0493	0.70699 ± 3	0.70680	+ 37
ZHB	Q–andesite	CHAR 6	279	2.36	13	0.1095	0.512546 ±11	+ 1.3	66	181	1.057	0.70823 ±10	0.70404	– 2
ZHB	Q–microdiorite	CHAR 1	279	4.09	195	0.1268	0.512536 ±05	+ 0.5	79	326	0.704	0.70789 ± 6	0.70509	+ 13
ZHB	Amphiboles	CHAR 1	279	12.3	55.6	0.1397	0.512606 ±04	+ 1.4	2.78	209	0.038	0.70545 ±10	0.70529	+ 16
Croix–de–Fer	Dacite	CCF 20	308	6.33	31.3	0.1222	0.512222 ±10	– 5.2	136	119	3.328	0.72319 ±32	0.70860	+ 63
Croix–de–Fer	Dacite	CCF 22	308	6.9	36.5	0.1152	0.512174 ±07	– 5.8	184	138	3.868	0.72309 ±12	0.70614	+ 28
Croix–de–Fer	Q–latiandesite	CCF 7	308	5	25.5	0.1187	0.512112 ±10	– 7.2	142	229	1.801	0.71740 ±03	0.70950	+ 76
Combeynot	Alkali granite	CO 5	312	5.72	19.8	0.1746	0.512477 ±21	– 2.2	277	27.6	29.373	0.81185 ±03	0.68142	–

lère Briançonnaise" and analyzed using laser-probe ^{40}Ar–^{39}Ar step heating of single grains. Laser probe experiments were performed using an instrument device that includes a MAP 215-50 noble gas mass spectrometer and a continuous 6W argon-ion laser operating in multimode (MONIÉ et al., 1997). Samples have been irradiated for 70 hours in the McMaster nuclear facility, together with several flux monitors including Mmhb-1 at 520.4 ± 1.7 Ma (SAMSON and ALEXANDER, 1987). During step-heating, the beam was defocused in order to get a diameter at least twice the size of the mineral being dated. The duration of heating for each step is typically of 30 seconds, followed by 5 minutes of gas cleaning and 15 minutes of isotopic measurements through 8 data sets on ^{36}Ar to ^{40}Ar. Blanks were monitored every three experiments and were in the range of 3×10^{-12}, 3×10^{-14}, 3×10^{-14}, 38.2×10^{-13} and 10^{-13} cc for m/z = 40, 39, 38, 37 and 36, respectively. Results were corrected for blanks, mass discrimination, radioactive decay of ^{39}Ar and ^{37}Ar, and neutron-induced interference reactions with Ca, K and Cl. Ages were calculated according to MCDOUGALL and HARRISON (1988) and were reported with one sigma uncertainty on Table 2. Ca/K ratios in amphiboles can be directly evaluated from the relation $Ca/K = 1.82 \times {}^{37}Ar_{Ca}/{}^{39}Ar_{K}$, whereas Cl/K is obtained from the relation $Cl/K = 0.22 \times {}^{38}Ar_{Cl}/{}^{39}Ar_{K}$.

3.2. MAJOR AND TRACE ELEMENT ANALYSIS

The main igneous facies of these suites were sampled and analyzed (Table 3). All the igneous mafic minerals are altered with the exception of amphiboles. The latter were separated from an andesite and diorite from ZBH. Trace element and Nd–Sr isotope analyses were performed on the less altered rock facies of these suites and purified hornblende separates.

Major and minor elements of the Combeynot granite and microgranite were analyzed by ICP-AES at the Centre de Recherche Pétrographique et Géochimique (CRPG) in Nancy. The other rocks were analyzed by XRF at the Laboratoire de Pétrographie of Claude Bernard University in Lyon.

Trace elements were analyzed by ICP-MS using two different techniques: acid dissolution or fusion with lithium borate, depending on the SiO_2 contents of the rocks. Trace elements of the SiO_2-rich rocks (SiO_2 = 60%) were measured at the Laboratoire de Géochimie of Paul Sabatier University in Toulouse, using lithium borate fusion, and following the procedures of VALLADON et al. (unpublished report): 100 mg of powdered rocks are weighted in a Pt crucible, with 320 mg Lithium metaborate and 80 mg Lithium borate (Fluka). After careful mixing of the powders, the crucible is heated for fusion at 1000 °C. After cooling, 8 ml double-distilled HNO_3 (12N) and HF are added for the dissolution of the glass. The final dilution to 30 ml of a 15 ml aliquot, with MilliQ™ water and after addition of internal standards (In-Re), corresponds to a total dilution of 3000. Detection limits are: REE and Y = 0.03 ppm, U, Pb and Th = 0.5 ppm, Hf and Nb = 0.1 ppm, Ta = 0.03 ppm, and Zr = 0.04 ppm.

The mafic rocks and hornblende separates were analyzed at the Laboratoire de Géodynamique des Chaînes Alpines of Joseph Fourier University in Grenoble, using acid dissolution and following the procedure of BARRAT et al. (1996). Detection limits are 0.01 ppm for REE.

3.3. STRONTIUM AND NEODYMIUM ISOTOPE ANALYSES

Before dissolution, the separated amphiboles were cleaned with HCl (2N) and washed using MillQ™ water (leaching method). The dissolution of 100 mg samples was done in closed Teflon® screw cap vessels with a HF–$HClO_4$ mixture and subsequently converted to chloride form using HCl (Table 4).

We used chemical separations of Rb/Sr and Sm/Nd based on the procedures of BIRCK and ALLÈGRE (1978) and RICHARD et al. (1976), respectively. Nd and Sr isotopic compositions were measured on a multicollector VG-sector mass spectrometer at the Laboratoire de Géochimie Isotopique of the Montpellier II University. Sr was loaded on single W filament previously covered with Ta and Nd was loaded on Re/Ta triple filaments. Repeated analyses of NBS987 and JMC361 standards gave average values of $^{87}Sr/^{86}Sr = 0.71023 \pm 4$ and $^{143}Nd/^{144}Nd = 0.51115 \pm 4$, respectively.

Isotopic data on hornblende and igneous rocks have been corrected for in situ decay with an age of 308 Ma (Croix-de-Fer samples), 311 Ma (Combeynot) and 279 Ma (ZHB, Guil).

4. Results

4.1. ^{40}Ar–^{39}Ar DATING OF THE INTRUSIVE ROCKS OF THE ZONE HOUILLÈRE BRIANÇONNAISE

Two amphiboles from the Chardonnet microdiorite and the Combarine andesite of the "Zone Houillère Briançonnaise" were dated, as well as a

biotite from one of the Croix de Fer dacites (CCF20). For the Chardonnet amphibole CHAR-1, the age spectrum is moderately convex (Fig. 3a) with a plateau date of 278.8 ± 6.6 Ma defined at the 2σ level for 75% of ^{39}Ar released. Ca/K and Cl/K ratios are respectively close to 22 and 0.1 for this portion of the spectrum, and higher in the first gas increments, corresponding to older apparent ages. The age pattern of the second amphibole V1B1 is more discordant than the previous one (Fig. 3b). The first heating steps have minimum ages ranging from 35 to 54 Ma, Ca/K ratios close to 4, and a mean Cl/K of 0.06. For the last 69% of ^{39}Ar released, apparent ages drop to a plateau date of 269.7 ± 5.6 Ma (2σ) corresponding to constant Ca/K values of 25, and Cl/K ratios of 0.37. This isotopic pattern can be interpreted to reflect the degassing of two different argon reservoirs, one released at low experiment temperature, related to the degassing of micro structural defects and inclusions (phyllites?), the second being representative of the true argon signature in the amphibole.

Biotite from dacite CCF20 produces a very discordant age spectrum (Fig. 3c), with a convex profile. Maximum ages close to 180 Ma are displayed by the central part of the spectrum, whereas younger dates are observed on both sides. Cl/K ratios record an evolution that is antithetical to the age spectrum, the lowest Cl/K being correlated with the oldest dates. These isotopic signatures suggest that argon was released from two reservoirs, most probably represented by two phyllite components, magmatic biotite and late Alpine chlorite interlayered with biotite. Convex or hump-shaped age spectra have been previously reported for samples containing more than one generation of micas (WIJBRANS and MCDOUGALL, 1986). In the present situation, the age spectrum of biotite CCF20 cannot be used to assess an age for magmatism or Alpine overprint.

4.2. ALTERATION AND ELEMENTAL MOBILITY

Our trace element study is based on "hygromagmaphile" trace elements (such as Th, Ta, La, Zr, Hf) (TREUIL, 1973; BOUGAULT, 1980; BOUGAULT et al., 1985), since these elements constitute appropriate geochemical tracers and remain generally largely immobile during alteration and metamorphism. It is generally admitted that calcite-rich rocks have anomalous Light Rare Earth Elements (LREE) enrichments (LUDDEN and THOMSON, 1979; HUMPHRIS, 1984). No calcite filling-veins have been observed in the studied volcanic rocks. Thus, we assume that LREE were not mobilized.

The altered nature (up to low grade greenschist facies) of the rocks means that before any petrological and geochemical inferences can be made from the chemistry of the rocks, the possible chemical effects of element mobility must be accounted for. Niobium is widely regarded as being immobile during low grade metamorphism of igneous rocks and has been plotted against some

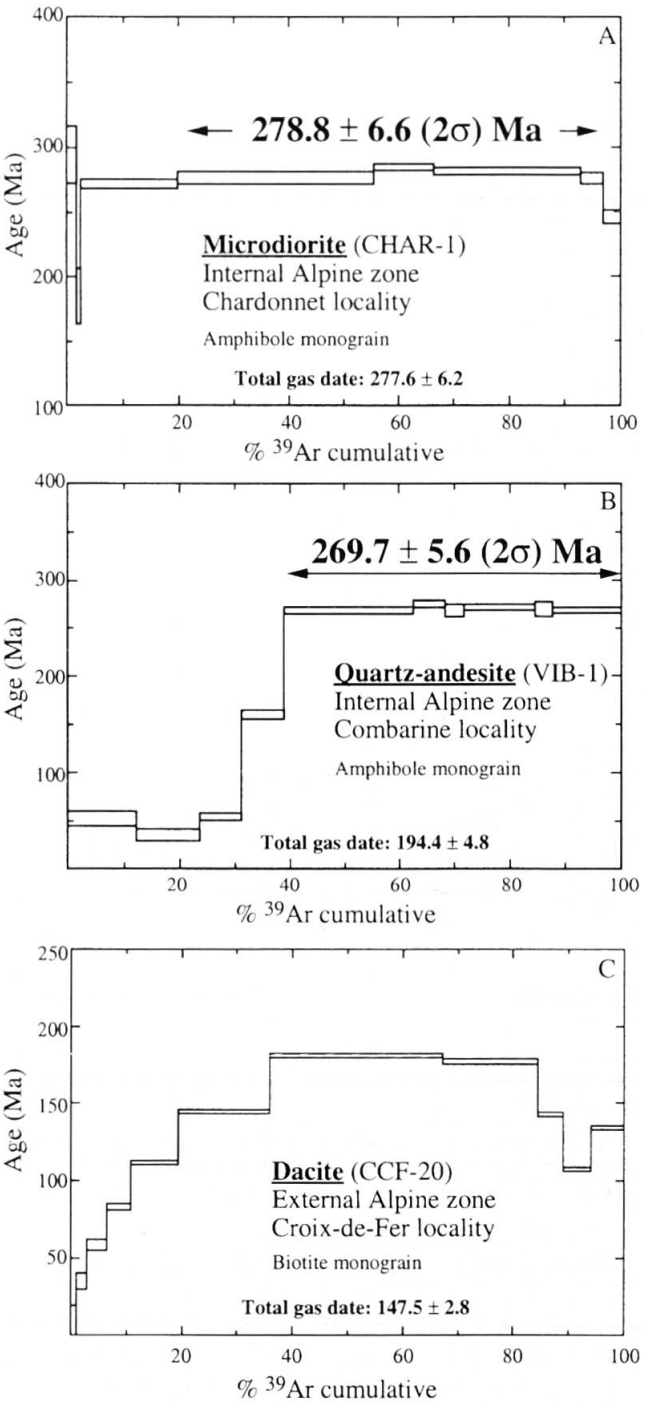

Fig. 3 Age spectra resulting from single grain analyses of microdiorite (CHAR1, A), quartz-andesite (VIB1, B) and dacite (CCF-20, C).

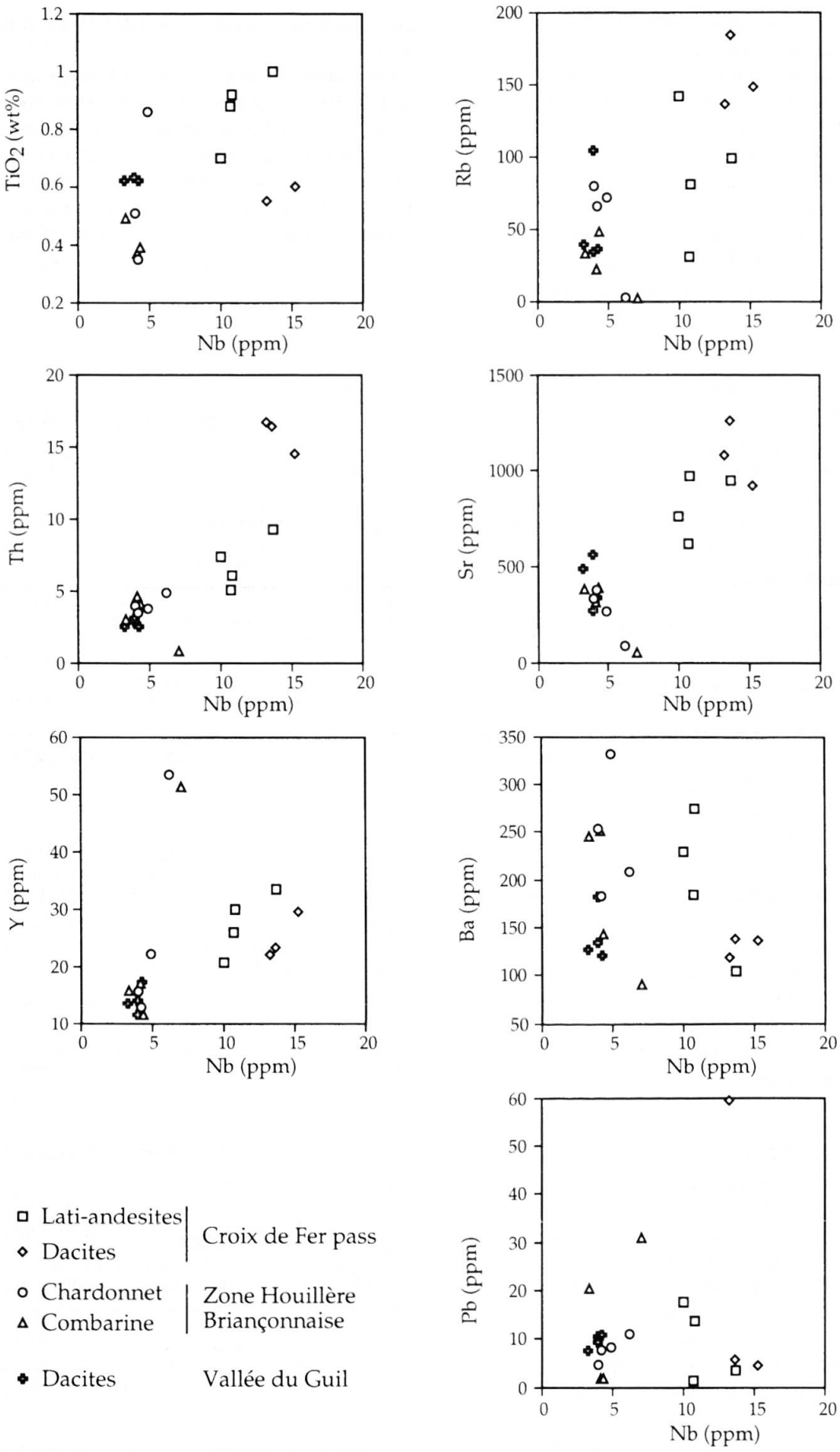

Fig. 4 Variations of minor- (TiO_2) and trace-element (Th, Y, Rb, Sr, Ba, and Pb versus Nb showing the mobility of large ion lithophile elements (LILE).

trace elements. It can be seen in Fig. 4 that Rb, Sr, Ba and Pb exhibit no correlation with Nb. This implies that these large ion lithophile elements have been extensively mobilized and that the Sr isotopic ratios do not reflect the compositions of the sources. The variations of these lithophile elements will not be discussed further on.

In contrast, TiO_2, Th and Y produce rather good correlations when plotted against Nb but these correlations differ slightly from one rock type to another. Most of the studied lavas exhibit an enrichment in TiO_2 and Y at rather similar Nb levels (5 and 10 ppm) with the exception of two dacites from the Croix de Fer pass. All the volcanic rocks display a crude Th–Nb positive correlation. This indicates that: (i) TiO_2, Y, and Th are relatively immobile during low grade metamorphism of the Permian–Carboniferous suites, and (ii) crystal fractionation is not the only process related to the differentiation of these rocks.

4.3. CROIX-DE-FER VOLCANISM

The major element composition (Table 3) of the lati-andesite ($SiO_2 < 55\%$), quartz-bearing andesite ($60\% < SiO_2 < 64\%$) and dacite ($SiO_2 > 65\%$) are in agreement with the petro-geochemical classification of BANZET et al. (1984). SiO_2 increases while Fe_2O_3 and TiO_2 decrease (refer to BANZET et al., 1984, 1985). This correlation is due to the early crystallizing ferro-titaneous oxides.

Among the studied suites (with the exception of the Combeynot granite), the lavas from the Croix-de-Fer have the highest Ta, Nb, Y, U and Th contents (Table 3). They cluster in the shoshonitic field defined by PEARCE (1982). Their Zr/Nb ($13 <$ Zr/Nb <15) and Zr/Th ($10 <$ Zr/Th < 24) ratios are high and fall in the range of shoshonitic suites (GILL, 1983; MORRISON, 1980). However, the dacite (CCF2) differs from the other lavas by significantly lower Zr/Nb (4.8) and Zr/Th (4.7) ratios, and falls in the calc-alkaline field (Fig. 5).

The Croix-de-Fer lavas are enriched in LREE relative to heavy rare earth elements (HREE). Their chondrite-normalized (SUN and MCDONOUGH, 1989) REE patterns fall in the range of shoshonitic suites (MÜLLER et al., 1992; $(La/Yb)_N$ ranging between 6.4 to 12.5, Table 3; Fig. 7A). The Croix-de-Fer lavas have negative Eu anomalies (Table 3; Fig. 7A), which are stronger in the most acidic rocks.

In order to study the differentiation of this suite, we have plotted the lavas (including data published by BANZET et al., 1985) in the Ce vs. La and Ce/Yb vs. Eu/Yb diagrams (HART and ALLÈGRE, 1980). Ce vs. La plot (Fig. 6A) shows a good positive correlation line that does not pass through the origin, corresponding to differentiation processes. However, CCF2 and CCF22 are the most LREE-enriched but have lower and higher Zr contents, respectively. This suggests that LREE-enrichment is not solely related to differentiation processes.

In the Ce/Yb vs. Eu/Yb plot, the Croix-de-Fer lavas show three trends (Fig. 6A). Trend 1 shows a positive correlation of Ce/Yb against Eu/Yb, which corresponds to fractionation of plagioclase. Trends 2 and 3 are parallel and indicate a Ce/Yb increase at given and different Eu/Yb ratios, related to frationation of amphibole and accessory phases.

The primitive mantle normalized spiderdiagrams (Fig. 8A) of the Croix-de-Fer lavas exhibit low field strenght elements (LFSE) enrichments and strong Nb, Ta and Ti negative anomalies.

The Croix-de-Fer volcanic rocks show a wide range of initial ε_{Sr} values (+34 to +79), while their ε_{Nd} are rather homogeneous and range between –5 to –7 (see Table 4). The ε_{Nd} ratio of the quartz-andesite is higher than that of the lati-andesite. In the ε_{Nd}–$(^{87}Sr/^{86}Sr)_i$ diagram (Fig. 9A), the Croix-de-Fer lavas plot out of the mantle array and are displaced to the right side of the diagram, towards the high ε_{Sr} values.

4.4. THE COMBEYNOT COMPLEX

The Combeynot granite and microgranite are SiO_2 (> 75%), K_2O (> 4.5%), and Fe_2O_3 (1 to 2%) rich and CaO (< 0.7%), MgO (< 0.8%) and Na_2O (< 4%) poor (Table 3). This indicates that they are formed from highly fractionated melts (COSTARELLA, 1987). Their Th levels are the highest of all the studied suites.

These SiO_2-saturated rocks have high HREE concentrations (20 and 30 times chondritic abundances) and show the lowest fractionation between LREE and HREE [$(La/Yb)_N < 5.4$; Fig. 7B] and marked negative Eu anomalies (Table 3). The greatest Eu negative anomaly is correlated with the lowest LREE-enrichment (CO5) and is possibly linked to allanite and feldspar removal (COSTARELLA, 1987). The REE patterns of these rocks are similar to those of hyper-alkaline granites (ALEKSIYEV, 1970; BOWDEN and WHITLEY, 1974). In the primitive mantle normalized spiderdiagram (Fig. 8B), these quartz-bearing rocks show Nb, Zr and Ti negative anomalies and Th and U enrichments.

The Combeynot shows an ε_{Nd} value of –2 and a very high $(^{87}Sr/^{86}Sr)_i$ which reflects the intense alteration that has affected this rock (Table 4).

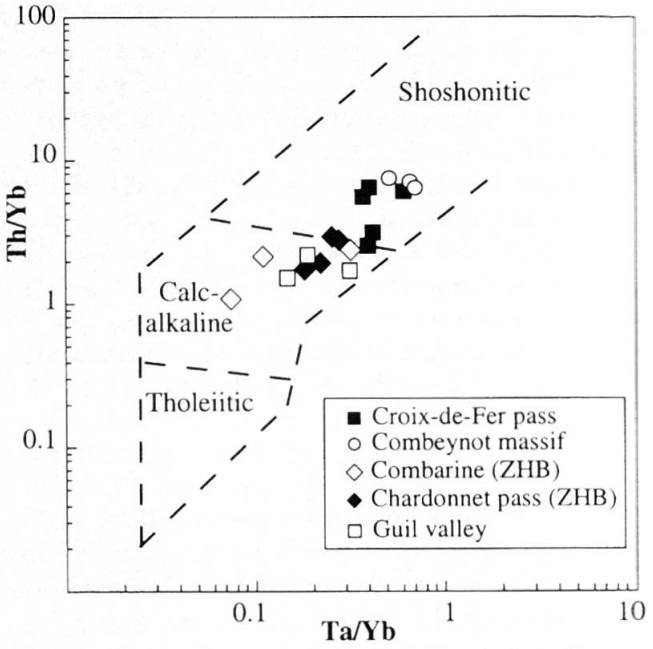

Fig. 5 Th/Yb–Ta/Yb discrimination diagram (after PEARCE, 1982 and MULLER et al., 1992) illustrating the shoshonitic to calc-alkaline affinities of the studied Permo-Carboniferous rocks.

4.5. ZONE HOUILLÈRE BRIANÇONNAISE MAGMATISM

The analyzed samples display a calc-alkaline affinity and a positive correlation between Th/Yb and Ta/Yb ratios (Fig. 5). They have high LREE contents and show an important fractionation between LREE and HREE [$(La/Yb)_N$ up to 5.6; Table 3; Fig. 7C and D]. The amphibole separates from a diorite porphyry (CHAR1) and an andesite (VIB1) differ from their host rocks by higher REE contents and Eu negative anomalies (Table 3; Fig. 7C). The CHAR1 amphibole (Fig. 7D) differs from that of VIB1 by a higher LREE enrichment relative to HREE [$(La/Yb)_N$ = 6.6 and 1.7, respectively] and a more marked Eu negative anomaly [Eu/Eu* = 0.7 and 0.8; Fig. 7D; Table 3]. The quartz-bearing diorites (COMB1 and COMB3) differ from the other ZHB rocks by Eu negative anomalies. This is confirmed in the Ce/Yb–Eu/Yb plot, where these two rocks have the highest Ce/Yb and Eu/Yb ratios (Fig. 6B). In the Ce–La and Ce/Yb–Eu/Yb plots the ZHB rocks show positive correlations.

In the primitive mantle-normalized spiderdiagram, diorites and diorite porphyries exhibit Nb, Ta and Ti negative anomalies and Th-, U-enrichments (Fig. 8C), which are, however, lower than those of the Croix-de-Fer suite. Relative to primitive mantle, the amphiboles share similar trace element distribution with their host rocks, but differ by the HREE and Y contents, which are lower in the host rocks. The ZHB rocks display a large range of U contents (35 to 105 times the primitive mantle abundances), while the range of their Th contents is restricted (between 3 and 4.7; Table 3). However, VIB1 amphibole has the highest U and lowest Th contents, respectively and thus, differs on this point from its host rock and the ZHB suite.

The studied rocks show rather homogenous initial ε_{Nd} values (+0.8 to +2.3), while their ε_{Sr} values are more variable and range from –5 to +39 (Table 3). VIB1 amphibole and its andesite host rock have similar ε_{Nd} of +2.3 but the ε_{Sr} of the amphibole is slightly higher (+37) than that of the host rock (+32). CHAR1 amphibole has higher ε_{Nd} (+1.7) and ε_{Sr} (+16) values than its host rock (ε_{Nd} = +0.6; ε_{Sr} = 11). In the ε_{Nd} – $(^{87}Sr/^{86}Sr)_i$ plot (Fig. 9A), the samples from Chardonnet fall in the mantle array, while the amphibole and their host rocks from the Combarine area (VIB1 and COMB3 in Table 4) have higher ε_{Sr} values (+32 to +39) and plot out of the mantle array.

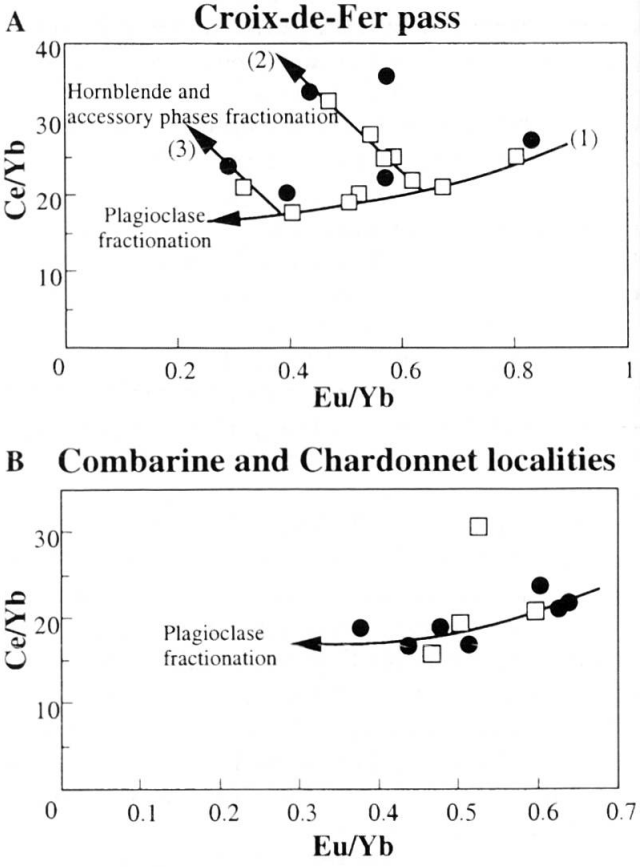

Fig. 6 Ce/Yb–Eu/Yb diagram (after HART and ALLÈGRE, 1980) for the Croix de Fer and Zone Houillère Briançonnaise igneous rocks. Open squares: data from BANZET et al. (1985). Full circles: this study.

4.6. GUIL VALLEY VOLCANISM

The rhyodacites and their inclusions of the Guil valley show a calc-alkaline affinity (Fig. 5). The analyzed samples display a constant Th/Yb ratio, similar to that of the ZHB rocks.

The felsic lavas and inclusions show similar chondrite-normalized patterns with a marked fractionation between LREE and HREE [$(La/Yb)_N$ = 5.2 to 6.1; Fig. 7E; Table 3]. However, the slightly more mafic xenoliths exhibit the lowest LREE enrichment relative to HREE [$(La/Yb)_N$ = 4.4]. Relative to primitive mantle, both rocks display similar Nb, Ta and Ti negative anomalies (Fig. 8D) and enrichments in Th and U.

The rhyodacites and inclusions show homogeneous ε_{Nd} values (+0.3 to +1.8), which are very similar to those of the ZHB rocks (Table 3). In the ε_{Nd} versus $(^{87}Sr/^{86}Sr)_i$ diagram (Fig. 9A), the rhyodacite (GUB3) falls in the mantle array, while the dioritic porphyry xenolith (GUB5) plots left of the mantle array because of its negative ε_{Sr} value. This negative ε_{Sr} is probably due to the very low ^{87}Rb and high ^{86}Sr contents (Table 3) of this rock and may reflect an alteration process.

4.7. SUMMARY AND DISCUSSION ON THE GEOCHEMISTRY OF THE LATE CARBONIFEROUS–EARLY PERMIAN SUITES

The Late Carboniferous and Early Permian igneous rocks of the External Alps share in common high $(La/Yb)_N$ ratios, and in primitive mantle-normalized plot, Nb, Ta and Ti negative anomalies and U and Th enrichments. The Late Carboniferous suite from the Croix-de-Fer pass differs from the ZHB and Guil rocks by higher contents in U, Th and REE. Finally, the lavas from the Croix-de-Fer pass and the Combeynot granite have negative ε_{Nd} values while those of the ZHB intrusives and Guil lavas range between +0.2 to +2.3.

The differentiation of the Croix-de-Fer suite appears to be very complex. Indeed, the quartz-andesites and the lati-basalts do not display significant differences in their Hf, Nb, Ta and REE abundances. This indicates that the most felsic rocks cannot derive from the basalts by crystal fractionation.

Differentiation of the ZHB rocks appears to be simplier than that of the Croix-de-Fer suite. VIB1 amphibole and its andesitic host rock differ from CHAR1 amphibole and its dioritic porphyry by lower Zr and HREE contents and Eu/Eu* ratio. This can be explained by the accumulation in the diorite porphyry of abundant plagioclase and zircon, which does not occur in the andesite. So, the chemical differences observed in the two amphiboles of the ZHB intrusives indicate that plagioclase played a key role in the differentiation of the ZHB intrusive rocks. The ε_{Nd} values of the VIB1 amphibole and its andesitic host rock are higher than that of CHAR1 amphibole and its diorite porphyry host rock. Similarly, the ε_{Nd} value of CHAR1 amphibole is slightly higher than that of its host rock. These differences in the ε_{Nd} values can be easily explained in terms of crustal assimilation. The cooling and differentiation of the diorite porphyry which forms the core of the dyke or sill, lasted longer compared to that of the andesitic chilled margin. During this differentiation and/or cooling, the amphibole and its host diorite porphyry may have assimilated crustal material, represented by the Carboniferous sediments, which form the wall rocks of the intrusion. In contrast, the ε_{Sr} value (+16) of the CHAR1 amphibole is higher than that of its host rock (ε_{Sr} = +13). This indicates that the Sr isotopic composition of these rocks is not significant.

The felsic rocks from the Guil valley are geochemically similar to the ZHB andesites and diorite porphyries, similar $(La/Yb)_N$ ratios, U and Th contents and ε_{Nd} ratios (Tables 3 and 4; Fig. 8D and 9A). The dacite differs from the tuff and diorite porphyry inclusion by a slightly higher ε_{Nd} value. This difference is likely linked to crustal contamination or assimilation.

5. Origin of the Late Carboniferous – Early Permian suites from the Western Alps

5.1. ORIGIN OF THE GEOCHEMICAL FEATURES OF THESE SUITES

The Late Carboniferous–Early Permian suites from the western Alps show features of subduction-related magmas which are commonly found in convergent-plate environments or in extensional tectonic settings related to strike-slip faults. These suites are not unique and belong to the large K-rich igneous province emplaced in the European Variscan belt during the Late Carboniferous–Early Permian times. The origin of this magmatism is still a matter of debate. For some authors (STAMPFLI, 1996), these K-rich magmas emplaced in a back-arc extensive setting related to the roll-back of the subducting paleo-Tethyan slab. For others (INNOCENT et al., 1994; FAURE, 1995; ROTTURA et al., 1998), these magmas were emplaced in distensive basins during post-orogenic lithospheric extension, which affected the entire European Variscan belt. In the External Crystalline Massifs, French Massif Central and in the Pyr-

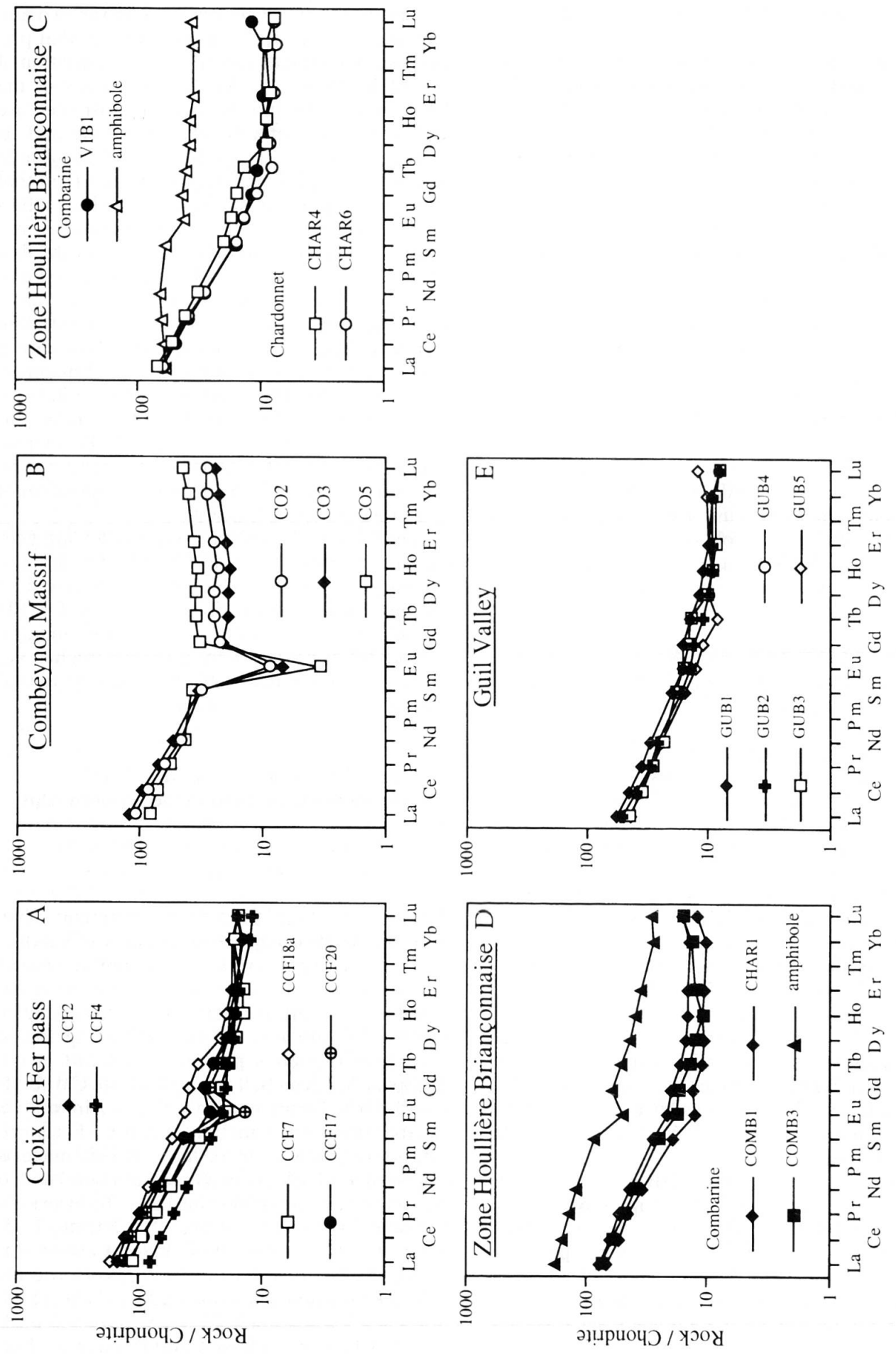

Fig. 7 Chondrite-normalized rare earth patterns (SUN and MCDONOUGH, 1989) for the studied Permo-Carboniferous rocks.

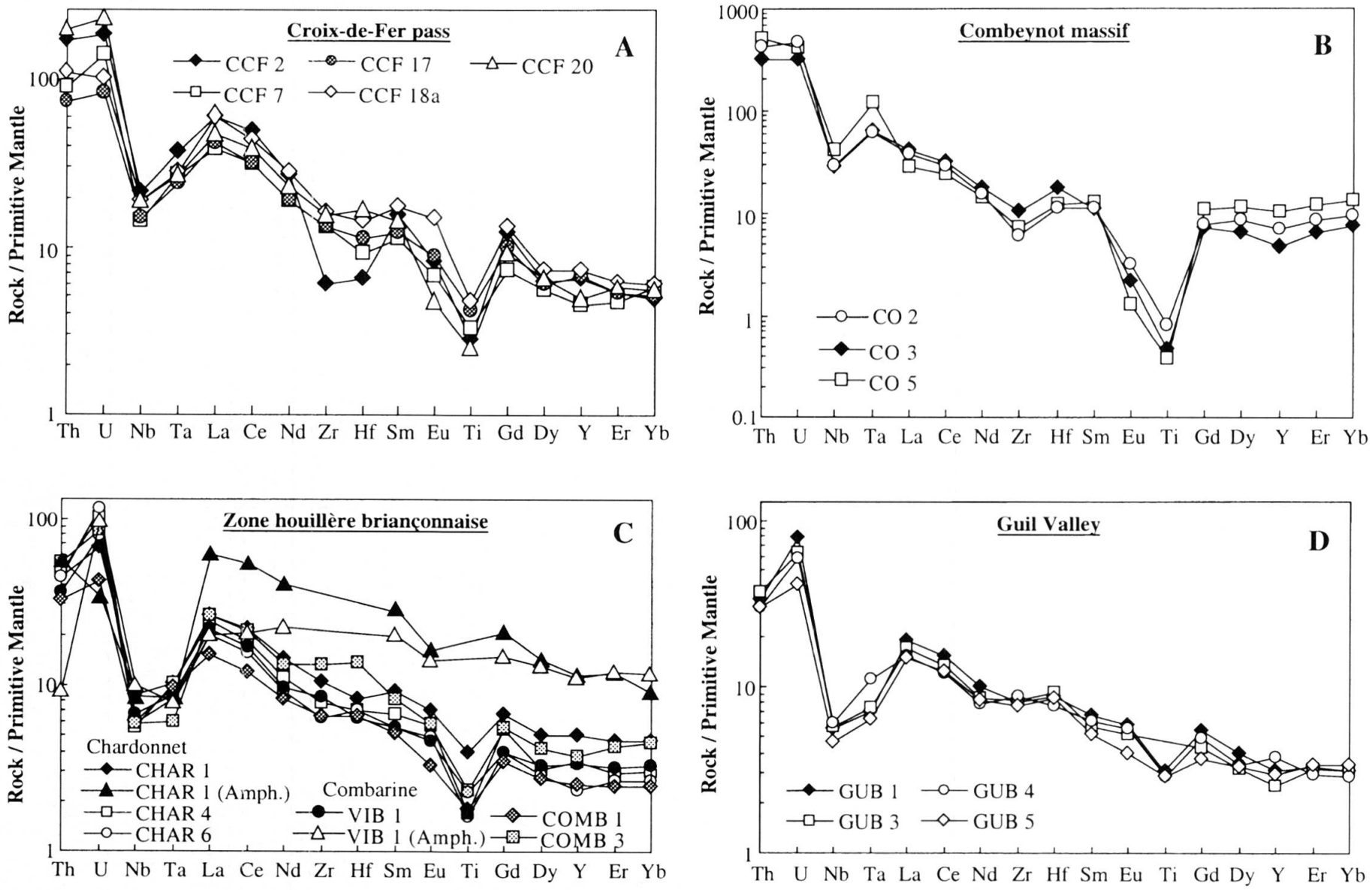

Fig. 8 Primitive mantle-normalized spidergrams (SUN and MCDONOUGH, 1989) for the studied Permo-Carboniferous rocks. Note the persistent negative anomalies of Nb, Ta and Ti and the Th and U enrichments.

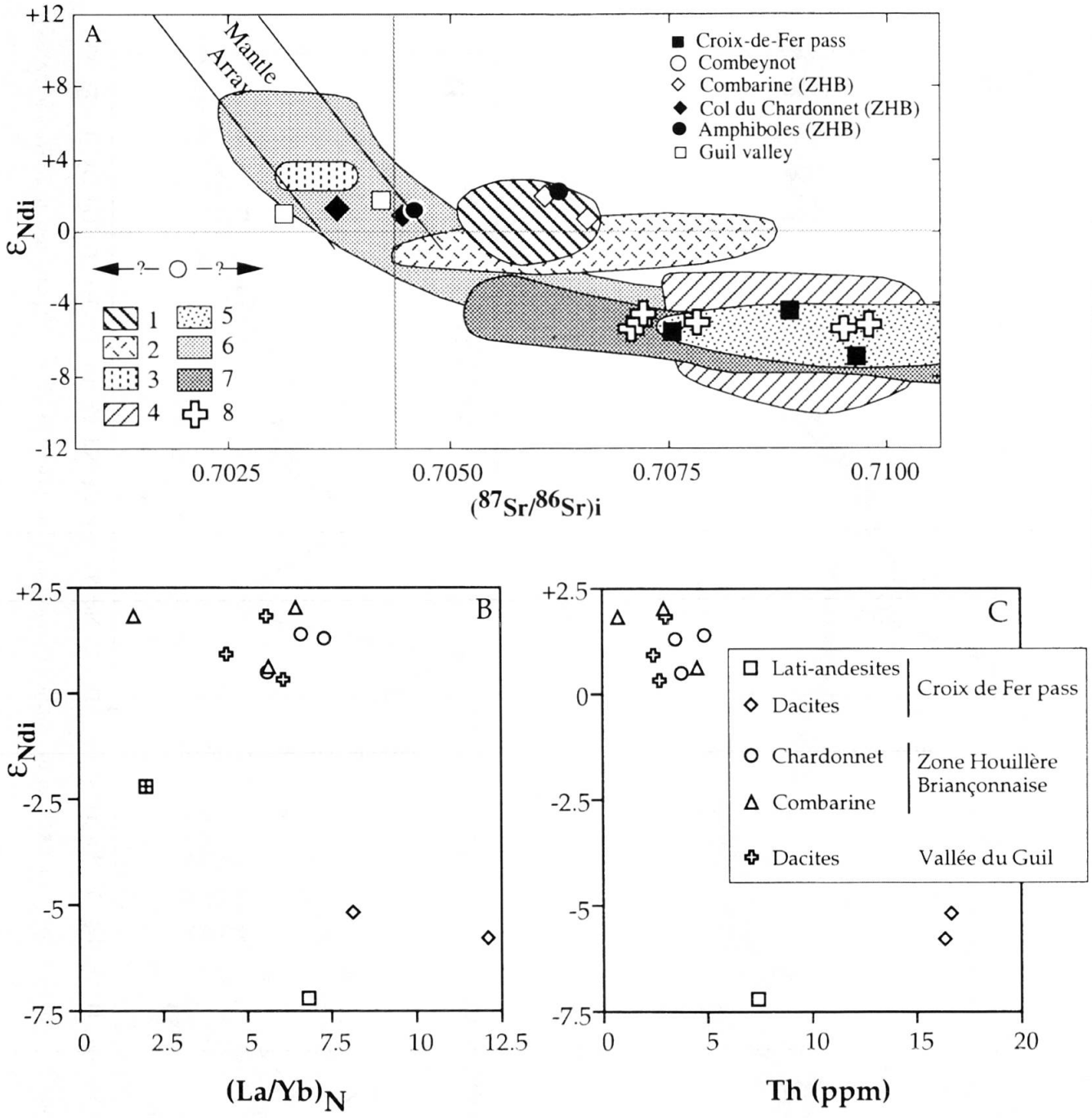

Fig. 9 ε_{Ndi} vs. $(^{87}Sr/^{86}Sr)i$ (A), $(La/Yb)_N$ (B) and Th (C) correlation diagrams for the studied Permo-Carboniferous rocks. Shown for comparison are the fields of: 1 – Triassic continental tholeiite (western Pyrenees; ALIBERT, 1985). 2 – Upper Permian La Rhune basalt (Pyrenees, INNOCENT et al., 1994). 3 – Mid-Permian Anayet andesite (Pyrenees, INNOCENT et al., 1994). 4 – Late Carboniferous Sierra del Cadi and Ossau massif volcanism (Pyrenees, INNOCENT et al., 1994). 5 – Carboniferous Decazeville basin volcanism (Massif Central, BERLY, unpublished data). 6 – Early Permian Ivrea mafic complex, western Alps (VOSHAGE et al., 1990). 7 – Permian andesites and dacites from central-eastern Southern Alps (ROTTURA et al., 1998). 8 – Upper Permian Lugano volcanic rocks (STILLE and BULETTI, 1987).

enees, some of these basins are clearly related to strike-slip faults (ARTHAUD and MATTE, 1977; BIXEL and LUCAS, 1983; CAPUZZO and BUSSY, 1998).

The Carboniferous igneous suites from the Alps (suites studied in this paper, Aar massif; SCHALTEGGER et al., 1991; SCHALTEGGER and CORFU, 1995), and the French Central Massif (BERLY et al., 1998; unpublished data), and the Lower Permian lavas from the Pyrenees (Ossau and Sierra del Cadi; INNOCENT et al., 1994) and Southern Alps (ROTTURA et al., 1998) are geochemically similar. Indeed, all these rocks display Ta, Nb and Ti negative anomalies, Th and U enrichments (relative to primitive mantle), LREE-enriched patterns (Fig. 10) and negative ε_{Nd} values (–3 to –7; Fig. 9A).

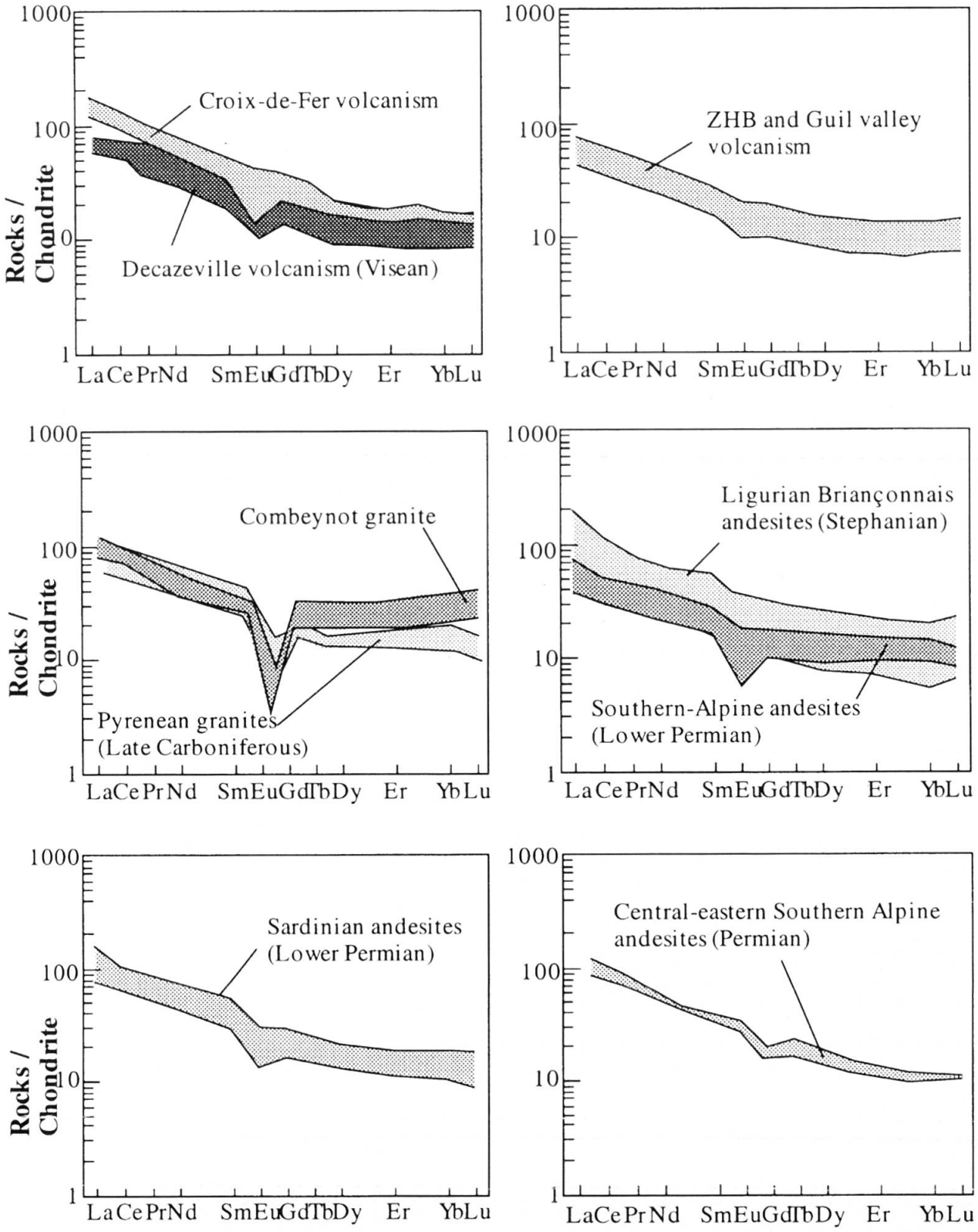

Fig. 10 Chondrite-normalized rare earth patterns (SUN and MCDONOUGH, 1989) for some Permo-Carboniferous magmatic suites. French Massif Central (Decazeville volcanism, BERLY et al., 1998); Ligurian Alps and Sardinia (CORTESOGNO et al., 1998); Pyrenees massifs (Querigut and Canigou; FOURCADE and ALLÈGRE, 1981).

The ZHB Early Permian intrusive rocks and the Guil dacites can be compared to the Upper Permian basalts (La Rhune) from the Pyrenees because their $^{143}Nd/^{144}Nd$ isotopic compositions are more or less similar ($-2 < \varepsilon_{Nd} < +2$; Fig. 9A). Moreover, these French suites are geochemically similar to the Stephanian and Lower Permian Italian suites because they are depleted in Nb and Ta (relative to the primitive mantle) and have high LREE/HREE ratios (Fig. 10). However, the

Lower Permian rocks from the External Alps are calc-alkaline while the La Rhune basalts are alkalic (INNOCENT et al., 1994).

The intrusive rocks from the Zone Houillère Briançonnaise and the dacites from the Guil valley display a crude negative correlation between the ε_{Nd} and Th content or $(La/Yb)_N$ ratio (Fig. 9B and C). Within the Permian rocks, those with the lowest ε_{Nd} values have the highest Th content and $(La/Yb)_N$ ratio. Similarly, among the studied suites, the Carboniferous volcanic rocks of the Croix de Fer pass which are the most Th- and LREE-enriched have the lowest ε_{Nd} values (Fig. 9B and C). This suggests involvement of continental crust in the genesis of these rocks.

Comparison between these different late Paleozoic suites shows that the magmatic affinities and isotopic compositions are not constrained by the age of the magmatism but rather by their paleogeographic distribution. However, in the Alpine arc, magmatism shows an evolution with time. The Late Carboniferous lavas show crustal signatures (negative ε_{Nd}), while the Early Permian intrusives clearly derive from the mantle, probably reflecting a change in crustal thickness.

Moreover, the Nb and Ta negative anomalies (in primitive mantle-normalized plot) of the late Paleozoic rocks from the external Alps are independent of their magmatic affinities and Nd isotopic compositions. This suggests that the lower continental crust, known to be depleted in Nb and Ta, is involved in the genesis of these rocks. Indeed, the lower continental crust normalized (WEAVER and TARNEY, 1984) patterns of the igneous suites from the external Alps do not show any enrichment or depletion in Nb, Ta, and Hf (Fig. 11A). In contrast, they are enriched in Th, HREE and Y. The Combeynot granite differs from the other suites, by a depletion in Zr, Eu and Ti. When normalized to the upper crust (TAYLOR and MCLENNAN, 1981) the patterns of the calc-alkaline and shoshonitic rocks have a depletion in Nb and Ta which is less marked in the Combeynot granite (Fig. 11B).

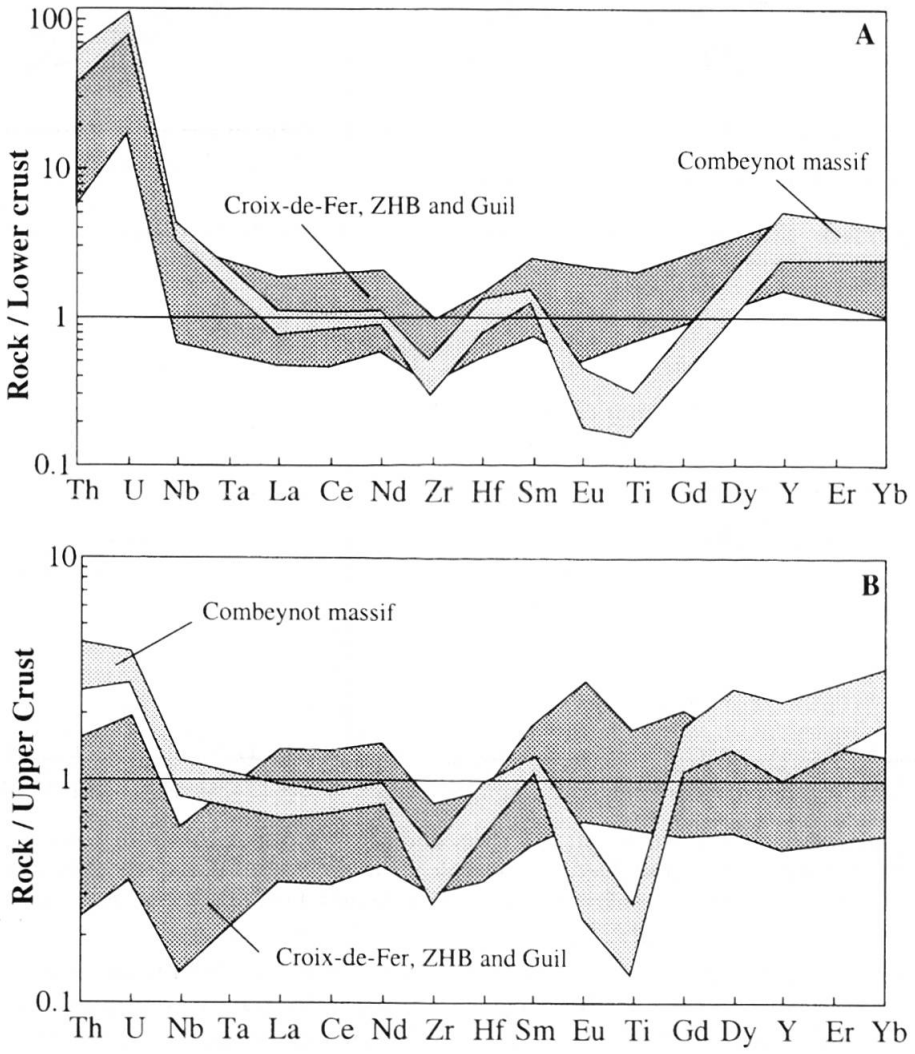

Fig. 11 (A) Lower and (B) upper crust-normalized spidergrams (WEAVER and TARNEY, 1984; TAYLOR and MCLENNAN, 1981, respectively) for the Croix de Fer and the Combeynot igneous suites.

All these rocks belong to calc-alkaline and/or shoshonitic suites, characterized by the absence of Ti and Fe enrichment during crystal fractionation. This is a feature of hydrous melts (GILL, 1981). The high water content in the magma is provided by the presence of amphibole and/or phlogopite in the mantle source or the mica-bearing gneiss present in the upper continental crust. The occurrence of an amphibole- or phlogopite-bearing metasomatosed mantle underlying the continental European crust at the end of the Variscan orogeny is most likely. Indeed, Ordovician subduction events are documented in the Paleozoic basement of the Alps, (e.g., U/Pb zircon ages on eclogites in the Gothard massif, OBERLI et al., 1994)

Thus, it appears on the basis of the trace element distribution and Nd isotopic compositions of the Late Carboniferous and Early Permian rocks, that these rocks originated through complex interactions between mantle-derived magmas and crustal material. However, it is difficult to specify the nature of the mantle source, i.e., subcontinental or asthenospheric.

5.2. GEODYNAMICAL IMPLICATIONS

Large-scale extension has been recognized in Europe at the end of the Variscan orogeny during the Late Carboniferous and Early Permian (BECQ-GIRAUDON and VAN DEN DRIESSCHE, 1994; BURG et al., 1994; FAURE, 1995). The Late Carboniferous event postdates the gravitational collapse of the Variscan chain and is related to transtensional extension, mainly controlled by strike-slip faults (ECHTLER and MALAVIEILLE, 1990; SAINT MARTIN et al., 1993; BARD, 1997). The Early Permian event is essentially related to extension (BROUTIN et al., 1994). Both events are likely related to a regime of lithospheric extension and thinning combined with gravitational collapse of the newly built Variscan chain induced by the change in the convergence direction between Gondwana and Laurasia (ARTHAUD and MATTE, 1977; ZIEGLER, 1993). This plate tectonic event affected the whole European Variscan belt. The Croix-de-Fer volcanism and Combeynot granite intrusion occurred during the first event and likely derived from the partial melting of the lower crust. During the Early Permian, the ZHB calc-alkaline shallow level intrusions and the Guil lavas emplaced in a thinned continental crust. These rocks derived from the partial melting of an enriched mantle, which experienced a small crustal contamination. Thus, the crustal contribution disappears progressively with time, corresponding to the progressive thinning of the lithosphere at the end of the Variscan orogeny. The latter being probably controlled the Mesozoic opening of the Tethyan ocean in this area.

6. Conclusions

The Late Carboniferous–Early Permian suites from Western Alps are characterized by:

(1) The Late Carboniferous shoshonitic volcanism of the Croix-de-Fer pass and alkaline Combeynot granite derive from the mixing between lithospheric mantle and lower crust components. However, crustal contamination was less important in the genesis of the Combeynot granite.

(2) The Early Permian age of calc-alkaline volcanism is confirmed by ^{40}Ar–^{39}Ar datations in the ZHB. This volcanism and the one from the Guil valley likely derived from an enriched mantle source which was affected by some crustal contamination.

The evolution of the nature of the magma sources with time, i.e. from the end of the Variscan orogeny up to the Early Permian magmatism, could be related to extension and thinning of the Variscan lithosphere.

Acknowledgments

This work was funded by GeoFrance 3D Alpes (contribution n° 119). G. Mevel (Centre de Recherche Pétrographique et Géochimique, Nancy), P. Capiez (Université C. Bernard, Lyon) and F. Keller (Université J. Fourier, Grenoble) are thanked for the chemical analyses. We would like also to thank F. Sénebier who did all the mineral separates. We are particularly grateful to F. Debon and F. Bussy, and two anonymous reviewers for their reviews and comments.

References

ALEKSIYEV, E.I. (1970): Genetic significance of the rare earth elements in the younger granites of northern Nigeria and Cameroon. Geochem. Int., 127–132.

ARTHAUD, F. and MATTE, P. (1977): Late Paleozoic strike-slipe faulting in southern Europe and northern Africa: results of right-lateral shear zone between the Appalachians and Urals. Geol. Soc. Am. Bull. 88, 1305–1320.

BANZET, G., ROUER, O. and LAPIERRE, H. (1984): Nouvelles données pétrographiques, stratigraphiques et structurales sur le volcanisme carbonifère du Col de la Croix-de-Fer (massifs cristallins externes, Alpes). Bull. Soc. géol. France 7, 1269–1280.

BANZET, G., LAPIERRE, H., LEFORT, P. and PECHER, A. (1985): Le volcanisme carbonifère supérieur du massif des Grandes Rousses (zone Dauphinoise, Alpes externes françaises): un magmatisme à affinités shoshonitiques lié à la fracturation crustale tardi-varisque. Géol. Alpine 61, 33–60.

BARBIÉRI, A. (1970): Étude pétrographique de la partie orientale du massif des Écrins-Pelvoux. Les granites.

Aperçu sur la géochronométrie du massif. Ph.D. Thesis, Grenoble, 127 pp.

BARD, J.P. (1997): Démembrement anté-mésozoïque de la chaîne varisque de l'Europe occidentale et de l'Afrique du Nord: rôle essentiel des grands décrochements transpressifs dextres accompagnant la rotation-translation horaire de l'Afrique durant le Stéphanien. C.R. Acad. Sci. Paris 324, 693–704.

BARFÉTY, J.C. and PECHER, A. (1984): Geological map 1:50'000, St-Christophe-en-Oisans. BRGM, Orléans.

BARRAT, J.A., KELLER, F., AMOSSÉ, J., TAYLOR, R.N., NESBITT R.W. and HIRATA, T. (1996): Determination of rare earth elements in sixteen silicate reference samples by ICP-MS after Tm addition and ion exchange separation. Geostandards Newsletter 32, 133–139.

BECQ-GIRAUDON, J.F. and VAN DEN DRIESSCHE, J. (1994): Dépôts périglaciaires dans le Stéphano-Autunien du Massif Central: témoin de l'effondrement gravitaire d'un haut plateau hercynien. C.R. Acad. Sci. Paris 318, 675–682.

BIRCK, J.L. and ALLÈGRE, C.J. (1978): Chronology and chemical history of the parent body of basaltic achondrites studied by the ^{87}Rb–^{87}Sr method. Earth Planet. Sci. Lett. 39, 37–51.

BIXEL, F. and LUCAS, C. (1983): Magmatisme, tectonique et sédimentation dans les fossés stéphano-permiens des Pyrénées occidentales. Rev. Geol. Dyn. Geogr. Phys., 24, 4, 329–342.

BONIN, B. (1980): Les complexes acides alcalins anorogéniques continentaux: l'exemple de la Corse. Ph.D. Thesis, Paris VI, 756 pp.

BONIN, B. (1982): Les granites des complexes annulaires. In: BRGM (eds), Manuels et méthodes, Orléans, 4, 183 pp.

BORDET, P. and CORSIN, P. (1951): Flore stéphanienne dans le massif des Grandes Rousses. C.R. somm. Soc. géol. Fr. 6, 73.

BOUGAULT, H. (1980): Contribution des éléments de transition à la compréhension de la génèse des basaltes océaniques. Ph.D. Thesis, Paris VII, 214 pp.

BOUGAULT, H., JORON, J.L., TREUIL, M. and MAURY, R. (1985): Local versus regional mantle heterogeneities: evidence from hygromagmatophile elements. Init. Rep. DSDP 82, 459–482.

BOWDEN, P. and WHITLEY, J.E. (1974): Rare-earth patterns in peralkaline and associated granites. Lithos 7, 15–27.

BROUTIN, J., CABANIS, B., CHATEAUNEUF, J.J. and DEROIN, J.P. (1994): Évolution biostratigraphique, magmatique et tectonique du domaine paléotéthysien occidental (SW de l'Europe): implications paléogéographiques au Permien inférieur. Bull. Soc. géol. France 2, 163–177.

BRUGUIER, O., BECQ-GIRAUDON, J.F., BOSCH, D. and LANCELOT, J.R. (1998): Late Visean (Upper Mississippian) hidden basins in the internal zones of the Variscan belt: U–Pb zircon evidence from the French Massif Central. Geology 26, 627–630.

BURG, J.P., VAN DEN DRIESSCHE, J. and BRUN, J.P. (1994): Syn- to post-thickening extension: mode and consequences. C.R. Acad. Sci. Paris 319, 1019–1032.

CABANIS, B. and LE FUR-BALOUET, S. (1989): Les magmatismes stephano-permiens des Pyrénées marqueurs de l'évolution géodynamique de la chaîne: apport de la géochimie des éléments en trace. Bull. Centres Rech. Explor. Prod. Elf-Aquitaine 13, 105–130.

CABANIS, B., COCHEMÉ, J.J., VELLUTINI, P., JORON, J.L. and TREUIL, M. (1990): Post-collisional Permain volcanism in north-western Corsica: an assessment based on mineralogy and trace element geochemistry. J. Volcanol. Geotherm. Res. 44, 51–67.

CAPUZZO, N. and BUSSY, F. (2000): High-precision dating and origin of synsedimentary volcanism in the Late Carboniferous Salvan-Dorénaz basin (Aiguilles-Rouges Massif, Western Alps). Schweiz. Mineral. Petrogr. Mitt. 80, 147–167.

COSTARELLA, R. and VATIN PÉRIGNON, N. (1985): An alkaline complex: The Combeynot massif in the French Alps. Terra Cognita 5, 318.

COSTARELLA, R. (1987): Le complexe annulaire alcalin de Combeynot (Massifs Cristallins Externes, Alpes françaises), témoin d'un magmatism en régime distensif. Pétrogéochimie et signification géodynamique. Ph.D. Thesis, Grenoble, 267 pp.

DE PAOLO, D.J. (1981): Trace element and isotopic effects of combined wallrocks assimilation and fractional crystallization. Earth Planet. Sci. Lett. 53, 189–195.

DEBON, F. and LEMMET, M. (1999): Evolution of Mg/Fe ratios in Late Variscan Crystalline Massifs of the Alps (France, Italy, Switzerland). J. Petrol. 40, 7, 1151–1185.

DEMEULEMEESTER, P. (1982): Contribution à l'étude radiométrique de l'argon et au strontium des massifs cristallins externes (Alpes françaises): distribution cartographique des âges sur biotites et amphiboles. Ph.D. Thesis, Grenoble, 227 pp.

ECHTLER, H. and MALAVIEILLE, J. (1990): Extensional tectonics, basement uplift and Stephano-Permian collapse basin in a late Variscan metamorphic core complex (Montagne Noire, Southern Massif Central). In: MATTE, P. (ed.): Terranes in the Variscan Belt of Europe and Circum-Atlantic Paleozoic Orogens. Tectonophysics 177, 125–138.

FAURE, M. (1995): Late orogenic Carboniferous extensions in the Variscan French Massif Central. Tectonics 14, 132–153.

FINGER, F. and STEYRER, H.P. (1990): I-type granitoids as indicators of Late Paleozoic convergent ocean-continent margin along the southern flank of the central European Variscan orogen. Geology 18, 1207–1210.

GILL, J. (1981): Orogenic andesites and Plate tectonics. Springer-Verlag, New-York, 390 pp.

GIORGI, L. (1979): Contribution à l'étude géologique des terrains cristallins du massif des Grandes Rousses. Isère, France. Ph.D. Thesis, Grenoble, 184 pp.

GOGUEL, J. (1966): Guillestre, feuille au 50'000 et notice explicative. BRGM, Orléans.

GREBER, C. (1965): Flore et stratigraphie du Carbonifère des Alpes françaises. Mém. BRGM 21, 380 pp.

HARRIS, N.B.W., PEARCE, J.A. and TINDLE, A.G. (1986): Geochemical characteristics of collision zone magmatism. In: COWARD, M.P., RIES, A.C. (eds): Collision Tectonics. Geol. Soc. Spec. Pub. 19, 67–81.

HART, S.R. and ALLÈGRE, C.J. (1980): Trace element constraints on magma genesis. Princeton University Press, Princeton, 121 pp.

HUMPHRIS, S.E. (1984): The mobility of rare earth elements in the crust. Rare earth elements geochemistry, P. HENDERSON, (ed.) Amsterdam, Oxford, New York, Tokyo, 510 pp.

INNOCENT, C., BRIQUEU, L. and CABANIS, B. (1994): Sr–Nd isotope and trace-element geochemistry of late Variscan volcanism in the Pyrénées: magmatism in post-orogenic extension? Tectonophysics 238, 161–181.

LACOMBE, J.C. (1970): Étude pétrographique de la partie orientale du massif des Écrins-Pelvoux. L'ensemble volcano-détritique. Ph.D. Thesis, Grenoble, 109 pp.

LAMEYRE, J. (1957): Le complexe volcanique de la partie nord du synclinal hercynien oriental du massif des

Grandes Rousses. C.R. somm. Soc. géol. Fr. 9, 105–149.

LUDDEN, J.N. and THOMSON, G. (1979): Behavior of rare earth elements during submarine weathering of tholeiitic basalts. Nature, 274,

MCDOUGALL, J. and HARRISON, T.N. (1988): Geochronology and thermochronology by the ^{40}Ar–^{39}Ar method. Oxford University Press, New York. Clarendon Press, Oxford. 212pp.

MÉNOT, R.P. (1987): Magmatisme paléozoïque et structuration carbonifère du massif de Belledonne (Alpes françaises). Contraintes nouvelles pour les schémas d'évolution de la chaîne varisque Ouest-Européenne. Ph.D. Thesis, Lyon, Rennes, 465 pp.

MERCOLLI, I. and OBERHÄNSLI, R. (1988): Variscan tectonic evolution in the central Alps: a working hypothesis. Schweiz. Mineral. Petrogr. Mitt. 68, 491–500.

MONIÉ P., CABY, R. and ARTHAUD, M.H. (1997): The Neoproterozoic Brasiliano orogeny in norteast Brazil, $^{39}Ar/^{40}Ar$ and petrostructural data from Ceara. Precamb. Res. 81, 241–264.

MORISSON, G.W. (1980): Characteristics and tectonic setting of the shoshonitic rock association. Lithos 13, 97–108.

MÜLLER, D., ROCK, N.M.S., GROVES, D.I. (1992): Geochemical discrimination between shoshonitic and Potassic volcanic rocks in different tectonic settings: a pilot study. Mineral. Petrol. 46, 259–289.

OBERLI, F., MEIER, M. and BIINO, G.G. (1994): Time constraints on the pre-Variscan magmatic/metamorphic evolution of the Gotthard and Tavetsch units derived from single-zircon U–Pb results. Schweiz. Mineral. Petrogr. Mitt. 74, 438–488.

ODIN, G.S. (1994): Geological time scale. C. R. Acad. Sci. Paris 318, 59–71.

OUAZZANI, H. and LAPIERRE, H. (1986): Le magmatisme carbonifère de la zone Briançonnaise (Alpes internes). Essai sur la lecture des magmatismes calco-alcalins tardifs dans les chaînes de collision continentale. C.R. Acad. Sci. Paris 302, 1171–1176.

OUAZZANI, H., BANZET, G. and LAPIERRE, H. (1987): Le volcanisme post-collision stéphanien à anté "permotriasique des Alpes françaises". Ann. Soc. géol. Nord CVI, 219–227.

PEARCE, J.A. (1982): Trace element characteristics of lavas from destructive plate boundaries. In: THORPE, R. S. (ed.), Andesites: Orogenic Andesites and Related Rocks, Wiley and sons, Chichester, London, 525–549.

PIANTONE, P. (1980): Magmatisme et métamorphisme des roches intrusives calco-alcalines du Carbonifère briançonnais entre Arc et Durance. Minéralogie, pétrographie, géochimie. Ph.D. Thesis, Grenoble, 214 pp.

RICHARD, P., SHIMIZU, N. and ALLÈGRE, C.J. (1976): $^{143}Nd/^{144}Nd$ a natural tracer. An application to oceanic basalts. Earth Planet. Sci. Lett. 31, 269–278.

ROLLINSON, H. (1993): Using geochemical data: evaluation, presentation, interpretation. Longman Scientific and Technical, 352 pp.

ROTTURA, A., BARGOSSI, G.M., CAGGIANELLI, A., DEL MORO, A., VISONÀ, D. and TRANNE, C.A. (1998): Origin and significance of the Permian high-K calc-alkaline magmatism in the central-eastern Southern Alps, Italy. Lithos 45, 329–348.

SAINT MARTIN, M., MALAVIEILLE, J. and MATTAUER, M. (1993): Gravity induced folding in late orogenic extensional basin (Graissessac Stephanian basin, Southern French Massif Central). In: SÉRANNE, M. and MALAVIEILLE, J. (eds): Late Orogenic Extension in Mountain Belts, Doc. BRGM, 170–171.

SAMSON, S.D. and ALEXANDER, E.C. (1987): Calibration of the interlaboratory $^{40}Ar/^{39}Ar$ dating standard MMhb-1. In: FAURE, G. (ed.): New developments and applications in isotope geosciences. 86, 27–34

SCHALTEGGER, U., GNOS, E., KÜPFER, T. and LABHART, T. P. (1991): Geochemistry and tectonic significance of Late Hercynian potassic and ultrapotassic magmatism in the Aar massif (Central Alps). Schweiz. Mineral. Petrogr. Mitt. 71, 391–403.

SCHALTEGGER, U. and CORFU, F. (1995): Late Variscan "Basin and Range" magmatism and tectonics in the Central Alps: evidence from U–Pb geochronology. Geodyn. Acta 8, 82–98.

STAMPFLI, G. (1996): The Intra-Alpine terrain: A Paleotethyan remnant in the Alpine Variscides. Eclogae Geol. Helv. 89, 13–42.

STILLE, P. and BULETTI, M. (1987): Nd–Sr isotopic characteristics of the Lugano volcanic rocks and constraints on the continental crust formation in the South Alpine domain (N-Italy-Switzerland). Contrib. Mineral. Petrol. 96, 140–150.

SUN, S. S. and MAC DONOUGH, W.F. (1989): Chemical and isotopic systematics of oceanic basalts: Implication for mantel composition and processes. Geol. Soc. Spec. pub. London. Magmatism in the ocean basin, 42, 313–345.

TAYLOR, S.R. and MCLEMMAN, S.M. (1981): The composition and evolution of the continental crust: rare earth element evidence from sedimentary rocks. Phil. Trans. R. Soc. A301, 381–399.

TREUIL, M. (1973). Critères pétrologiques, géochimiques et structuraux de la génèse et de la différenciation des magmas basaltiques. Exemple de l'AFAR. Ph.D. Thesis, Orléans, 170 pp.

WEAVER, B. and TARNEY, J. (1984): Empirical approach to estimating the composition of the continental crust. Nature 310, 575–579.

WIJBRANS, J.R. and MC DOUGALL, I. (1986): $^{39}Ar/^{40}Ar$ dating of white micas from an Alpine high-pressure metamorphic belt on Naxos (Greece); the resetting of the argon isotopic system. Contrib. Mineral. Petrol., 93, 187–194.

ZIEGLER, P.A. (1993): Late Paleozoic–Early Mesozoic Plate re-organization: evolution and demise of the Variscan Fold belt. In: VON RAUMER, J. and NEUBAUER, F. (eds): The pre-Mesozoic geology in the Alps, Springer-Verlag, Berlin, 171–201.

Manuscript received September 29, 2000; revision accepted January 7, 2002.
Editorial handling: J.D. Kramers